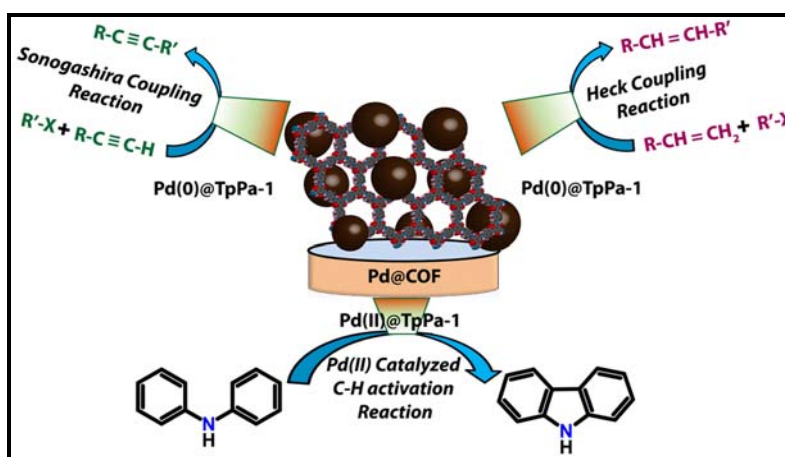


Supporting Information

Multifunctional and Robust Covalent Organic Framework-Nanoparticles Hybrids

Pradip Pachfule, Manas K. Panda, Sharath Kandambeth, S. M. Shivaprasad, David Díaz
Díaz, and Rahul Banerjee*



Information flow diagram of the Supporting Information

Synthesis and characterization of COF and catalyst

- S1. Experimental procedures, materials and methods
- S2. TpPa-1 synthesis
- S3. Pd(0)@TpPa -1 synthesis
- S4. Pd(II)@TpPa -1 synthesis

IR, elemental analyses, PXRD, SEM, TEM, EDAX, gas adsorption and XPS of COF and catalysts

Optimization of reaction conditions and products characterization

- S5. General procedures followed for catalytic reactions
- S6. Optimization of base, solvent, temperature, time and catalyst loading
- S7. Product characterization of Sonogashira coupling reactions
- S8. Product characterization of Heck coupling reactions
- S9. Product characterization of sequential Heck/Sonogashira coupling and oxidative biaryl synthesis reactions

Catalyst stability tests

- S10. 1) Pd leaching tests
- 2) Mercury drop test
- 3) Catalyst recyclability experiments
- 4) TEM and EDAX analysis of reused COF and AC supported catalysts
- 5) Carbon mass balance of the model reaction.
- 6) Thermogravimetric analyses of catalyst

Contents List

Section S1. Experimental procedures, materials and methods	4
Section S2. Synthesis and characterization of TpPa-1	6
Section S3. Synthesis and characterization of Pd(0)@TpPa-1	9
Section S4. Synthesis and characterization of Pd(II)@TpPa-1	14
Section S5. General procedures followed for catalytic reactions	20
Section S6. Optimization of reaction conditions:	22
1. Optimization of base	22
2. Optimization of solvent	23
3. Optimization of temperature, time and catalyst loading	24
4. Optimization of aryl halide	25
Section S7. Product characterization of Sonogashira coupling reactions	26
Section S8. Product characterization of Heck coupling reactions	32
Section S9. Product characterization of sequential Heck/Sonogashira coupling and intramolecular oxidative biaryl synthesis reactions	36
Section S10. Catalyst leaching, recyclability and stability tests	38
1. Pd-leaching tests	38
2. Mercury drop test	40
3. Catalyst recyclability experiments	41
4. TEM analyses of reused COF and AC supported catalysts	43
5. Carbon mass balance of the model reaction	45
6. Thermogravimetric analyses of Pd(0)@TpPa-1 and Pd(II)@TpPa-1	46
Section S11. References	47

Section S1. Experimental procedures, materials and methods:

All the reagents and solvents used for **TpPa-1** synthesis, catalyst preparation and catalytic reactions (i.e., Sonogashira, Heck, sequential Heck/Sonogashira cross coupling reactions and intramolecular oxidative biaryl coupling reactions) were commercially available and used as received.

PXRD, FT-IR, TGA, SEM, EDAX, TEM, NMR and XPS analyses:

Powder X-ray diffraction (PXRD) patterns were recorded on a Phillips PANalytical diffractometer for Cu K α radiation ($\lambda = 1.5406 \text{ \AA}$), with a scan speed of 1° min^{-1} and a step size of 0.02° in 2θ . Fourier transform infrared (FT-IR) spectra were taken on a Bruker Optics ALPHA-E spectrometer with a universal Zn-Se ATR (attenuated total reflection) accessory in the $600\text{-}4000 \text{ cm}^{-1}$ region or using a Diamond ATR (Golden Gate). Thermogravimetric analyses (TGA) were carried out on a TG50 analyzer (Mettler-Toledo) or a SDT Q600 TG-DTA analyzer under N $_2$ atmosphere at a heating rate of $10 \text{ }^\circ\text{C min}^{-1}$ within a temperature range of $30\text{-}900 \text{ }^\circ\text{C}$. SEM images were obtained with a Zeiss DSM 950 scanning electron microscope and FEI, QUANTA 200 3D. Scanning Electron Microscope with tungsten filament as electron source operated at 10 kV was used to get SEM images. The samples were sputtered with Au (nano-sized film) prior to imaging by a SCD 040 Balzers Union as well as by sprinkling the powder on carbon tape. Microscopy analyses were performed using a LEICA Stereoscan 440 scanning electron microscope (SEM) equipped with Phoenix energy dispersive analysis of X-ray (EDAX). To investigate the microstructure and morphology of the nanoparticles, we used the FEI (model Tecnai F30) high resolution transmission electron microscope (HRTEM) equipped with field emission source operating at 300 KeV to image the nano-crystals on carbon-coated copper TEM grids. The nanoparticles were dispersed in iPrOH and drop casted on the TEM grids. NMR data were taken on Bruker 200 and 400 MHz NMR spectrometers. X-Ray photoelectron spectroscopic (XPS) measurements were carried out on a VG Micro Tech ESCA 3000 instrument at a pressure of $>1 \times 10^{-9}$ Torr (pass energy of 50 eV, electron take-off angle of 60° , and overall resolution was 0.1 eV).

Gas adsorption and pore size distribution measurements:

Low pressure volumetric N $_2$ gas adsorption measurements involved in this work were performed at 77 K maintained by a liquid nitrogen bath, with pressures ranging from 0 to 760 Torr on Quantachrome Autosorb-iQ gas sorption device. In all the adsorption

measurements, ultra high-purity N₂ was obtained by using calcium aluminosilicate adsorbents to remove trace amounts of water and other impurities before introduction into the system. For the gas adsorption studies of **TpPa-1**, the solvent exchanged sample was dried under a dynamic vacuum ($<10^{-3}$ Torr) at room temperature (RT) overnight followed by heating at 100 °C for 12 h and 120 °C for 12 h under a dynamic vacuum. The completely dried samples (0.05 g) were loaded for gas adsorption study in the sample cells. The samples prepared by inclusion of Pd(0) nanoparticles and Pd(II) acetate into **TpPa-1** (i.e., **Pd(0)@TpPa-1**, **Pd(II)@TpPa-1**) were loaded for N₂ adsorption study as synthesized. The pore distributions plots were calculated using Quenched Solid Density Functional Theory (QSDFT) and Density Functional Theory (DFT) methods using the nitrogen adsorption isotherms obtained at 77 K and 1 atm pressure.

Inductively coupled plasma (ICP) Analysis:

The weight percentage loading of Pd on TpPa-1 COF in **Pd(0)@TpPa-1** and **Pd(II)@TpPa-1** have been analyzed using Inductively Coupled Plasma Optical Emission Spectrometry (ICP-OES) instrument from Spectro Arcos (Model No.: ARCOS-FHS-12; Input: 230 VAC 50/60 Hz; Part No.: 76004554). Samples for ICP analyses were prepared by using Aqua regia as a digesting solution. In a typical stock solution preparation, 2 mg of **Pd(0)@TpPa-1** and **Pd(II)@TpPa-1** was dissolved in 10 mL Aqua regia with sonication for 15 min. After complete dissolution of the catalyst, the solution was filtered through syringe filters (0.22 μL) in order to remove any insoluble impurities. The stock solution was further diluted with water to ppm level accordingly.

The obtained results from these analyses are as follows:

1. Pd(0)@TpPa-1 : 6.57 wt%
2. Pd(II)@TpPa-1: 10.08 wt%

Section S2. Synthesis and characterization of TpPa-1:

Triformylphloroglucinol was prepared from phloroglucinol following the procedure reported in the literature.¹

Synthesis and characterization of TpPa-1:

The synthesis of **TpPa-1** was performed according to the literature reported our recent communication.² Specifically, a pyrex tube (o.d. \times i.d. = 10 \times 8 mm² and length 18 cm) was charged with triformylphloroglucinol (**Tp**) (63 mg, 0.3 mmol), paraphenylenediamine (**Pa-1**) (48 mg, 0.45 mmol), mesitylene (1.5 mL), dioxane (1.5 mL), and aqueous acetic acid (0.5 mL from a 3 M solution). The mixture was sonicated for 10 minutes in order to get a homogenous dispersion. The tube was then flash frozen at 77 K (liquid N₂ bath) and degassed by three freeze-pump-thaw cycles. The tube was sealed off and heated at 120 °C for 3 days. A red *colored* precipitate formed was collected by centrifugation or filtration and washed with anhydrous acetone. The powder collected was then solvent exchanged with anhydrous acetone 5-6 times and then dried at 180 °C under vacuum for 24 h to give the product as a deep red colored powder in 80% isolated yield (89 mg).

IR (powder, cm⁻¹): 1585 (s), 1578 (w), 1450 (s), 1255 (s), 1096 (m), 992 (s), 824 (s)

Elemental analysis. For C₈₀O₁₂N₁₃H₄₈

Calculated: **C**, 69.5; **H**, 3.47; **N**, 13.87

Found: **C**, 68.4; **H**, 3.26; **N**, 13.56

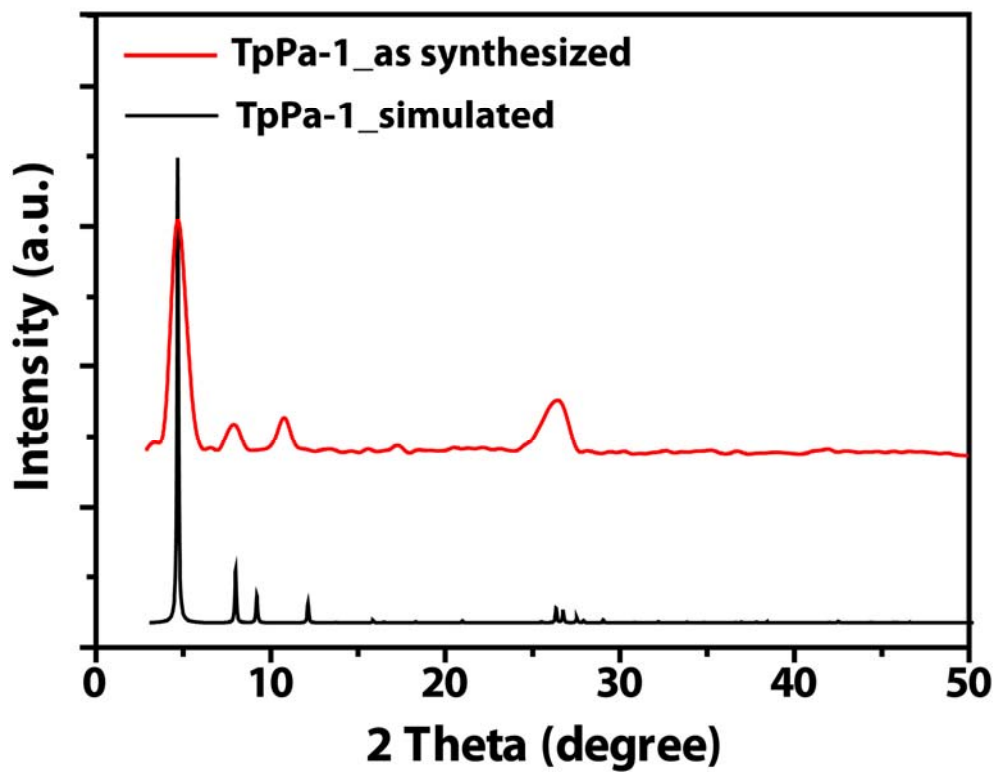


Figure S1. PXRD analysis of **TpPa-1** compared with the corresponding simulated pattern, showing peak to peak match with the bulk material.

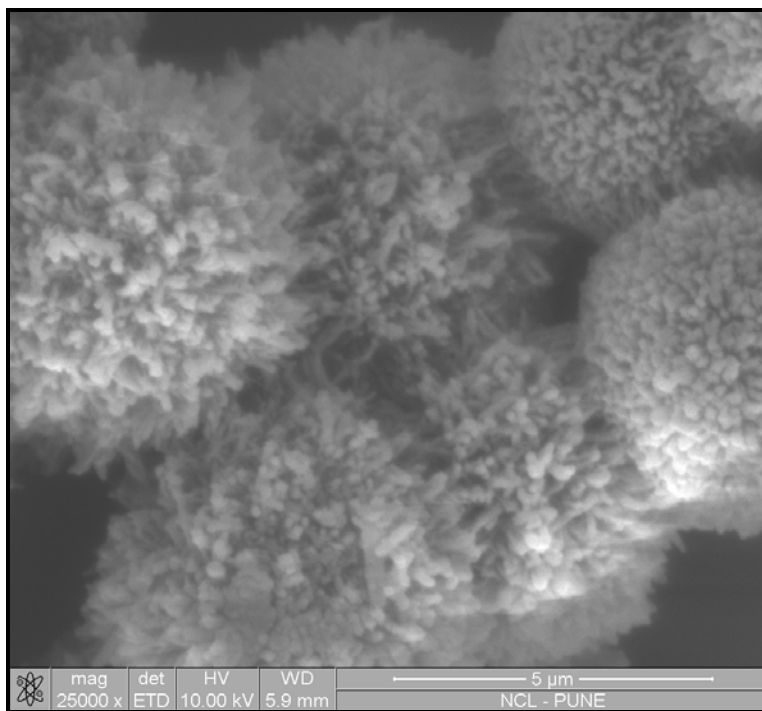


Figure S2. SEM image of the **TpPa-1** showing a flower-like morphology.

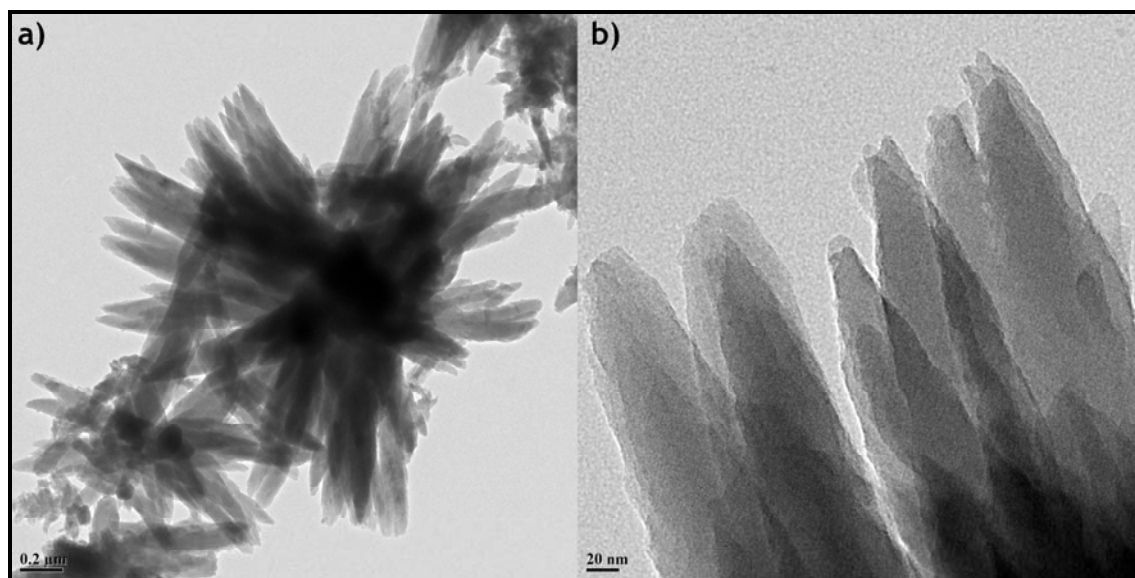


Figure S3. TEM images of **TpPa-1** after sonication in *i*PrOH. a) Low resolution TEM image of **TpPa-1** showing flower like morphology of COF. b) High resolution TEM image of **TpPa-1** showing arranged sheets.

Section S3. Synthesis and characterization of Pd(0)@TpPa-1:

In a typical synthesis of **Pd(0)@TpPa-1**, pre-synthesized and activated **TpPa-1** (100 mg) was dispersed in 5 mL of MeOH under ambient conditions, to which a MeOH solution (2 mL) containing Na_2PdCl_4 (15 mg, 0.07 mmol) was added dropwise under vigorous stirring. The mixture was evaporated until it became mushy. To this solution, 4 mL MeOH was subsequently added into the slurry, followed by a solution (3 mL) of NaBH_4 (2 M in MeOH) under vigorous stirring. After 30 min, the residue was recovered by filtration and thoroughly washed several times with MeOH (3×10 mL) to remove any impurity. The so prepared sample of **Pd(0)@TpPa-1** was further dried in a vacuum drying oven at 50 °C.

IR (powder, cm^{-1}): 1580 (s), 1568 (w), 1445 (s), 1251 (s), 1098 (m), 995 (s), 827 (s)

Elemental analysis. For **Pd(0)@TpPa-1**

Calculated: **C**, 64.77; **H**, 3.23; **N**, 12.92

Found: **C**, 63.6; **H**, 3.12; **N**, 12.07

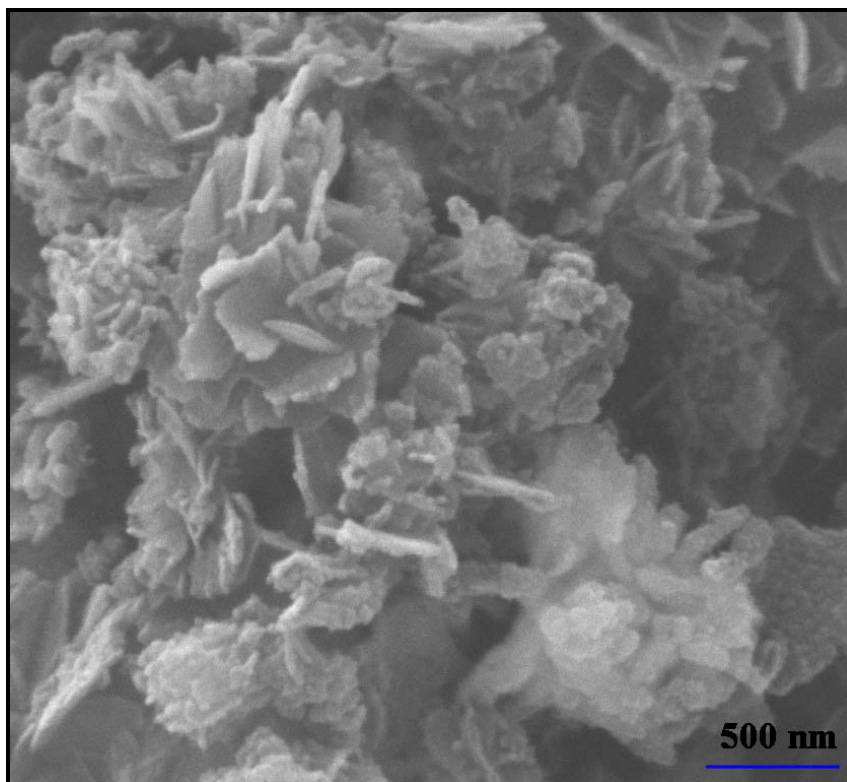


Figure S4. SEM image of the **Pd(0)@TpPa-1** showing the morphology of the **TpPa-1** after Pd(0) nanoparticle loading.

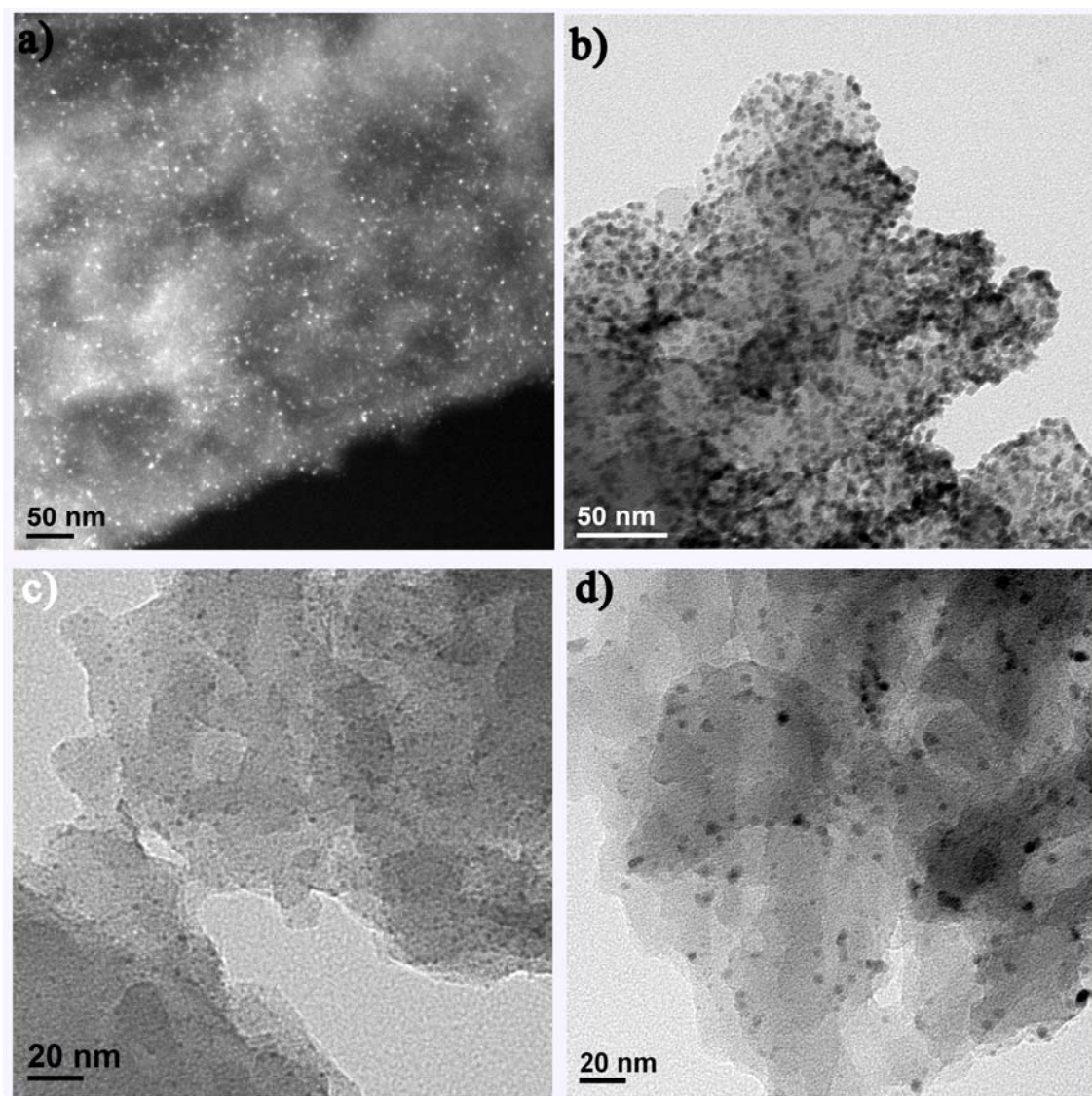


Figure S5. TEM images of **Pd(0)@TpPa-1**. a) Low resolution TEM image shows finely distributed 7 ± 3 nm sized Pd(0) nanoparticles distributed overall surface without agglomeration in dark field imaging. b) and c) Fine distribution of Pd(0) nanoparticles into the layered structure of **TpPa-1**, showing nicely separated Pd(0) nanoparticles loaded into the **TpPa-1** matrix. d) High resolution TEM image of Pd(0) nanoparticles homogeneously distributed on **TpPa-1**.

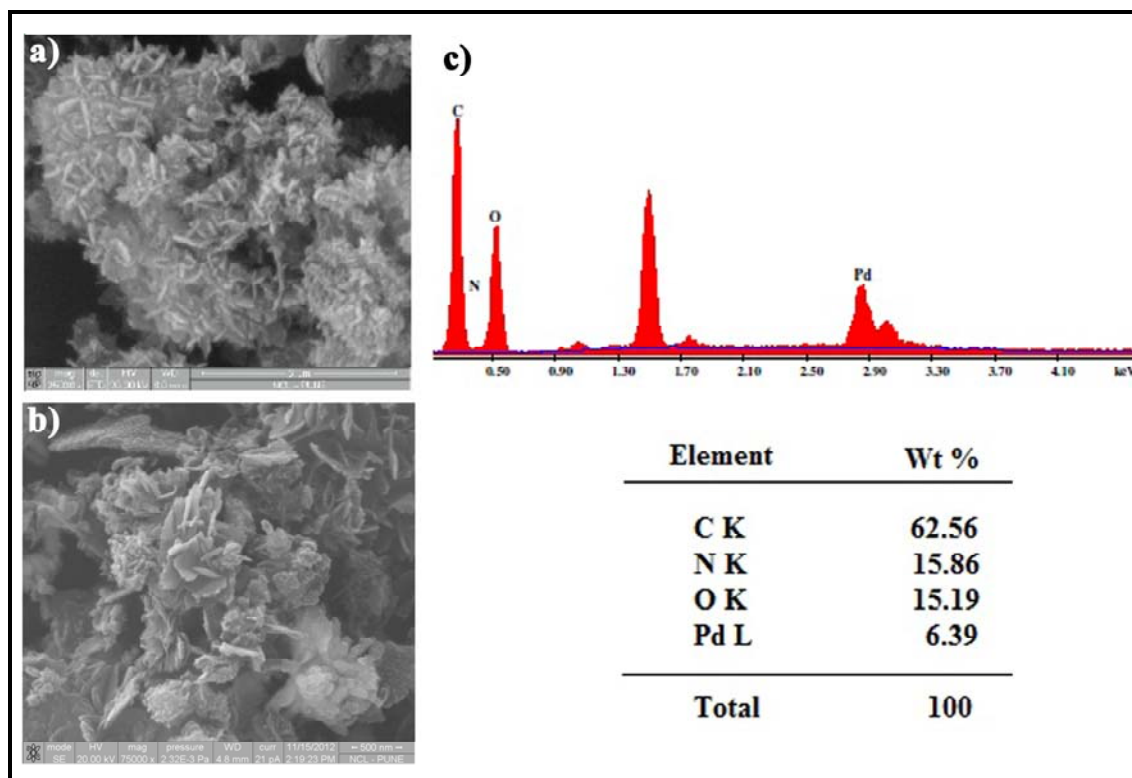


Figure S6. Comparative SEM images of **TpPa-1** and **Pd(0)@TpPa-1** and EDX analysis of **Pd(0)@TpPa-1**. a) SEM image of **TpPa-1** showing a flower-like morphology. b) SEM image of **Pd(0)@TpPa-1** showing maintained morphology of **TpPa-1** after loading of Pd(0) nanoparticles into the matrix. c) EDX analysis of **Pd(0)@TpPa-1** showing 6.3 wt.% loading of Pd(0) nanoparticles.

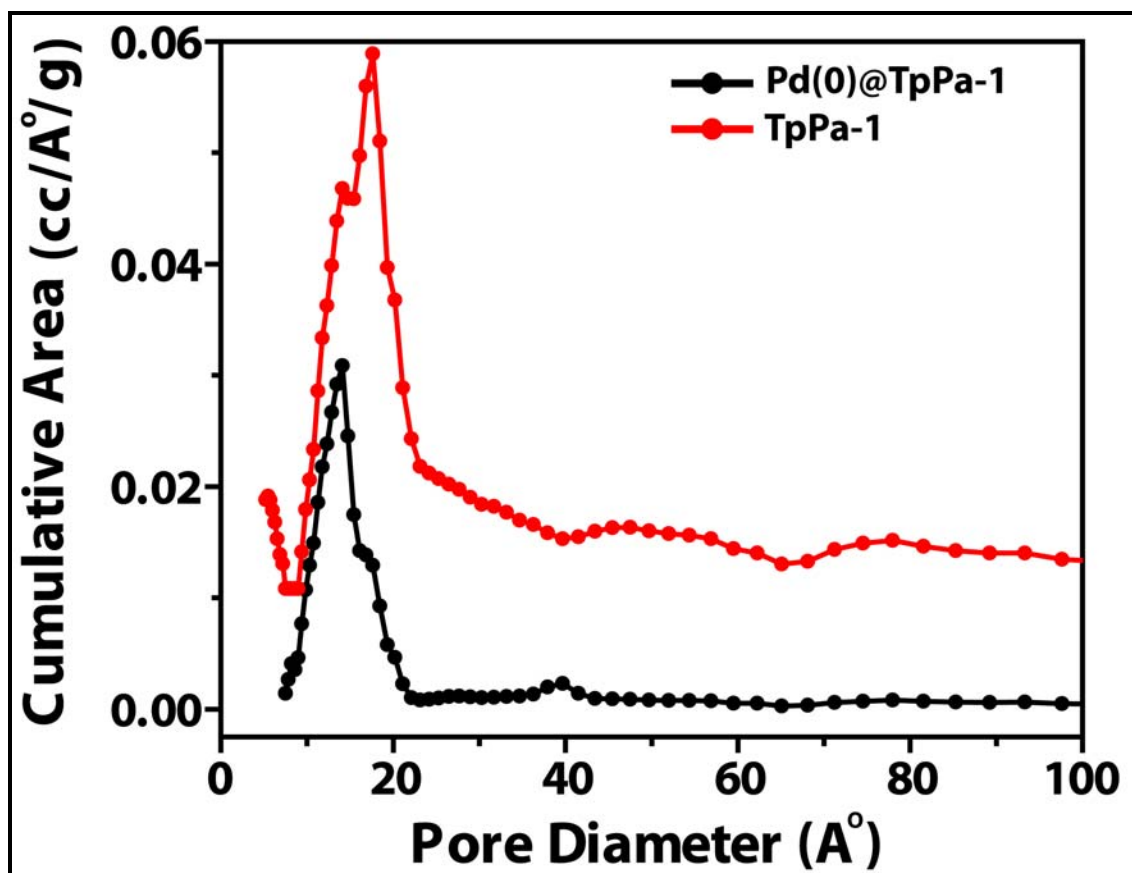


Figure S7. Pore size distribution analyses of **Pd(0)@TpPa-1** and **TpPa-1**. Density Functional Theory (DFT) pore size distribution plots for **TpPa-1** and **Pd(0)@TpPa-1** show decrease in the pore size of **Pd(0)@TpPa-1** after nanoparticle loading.

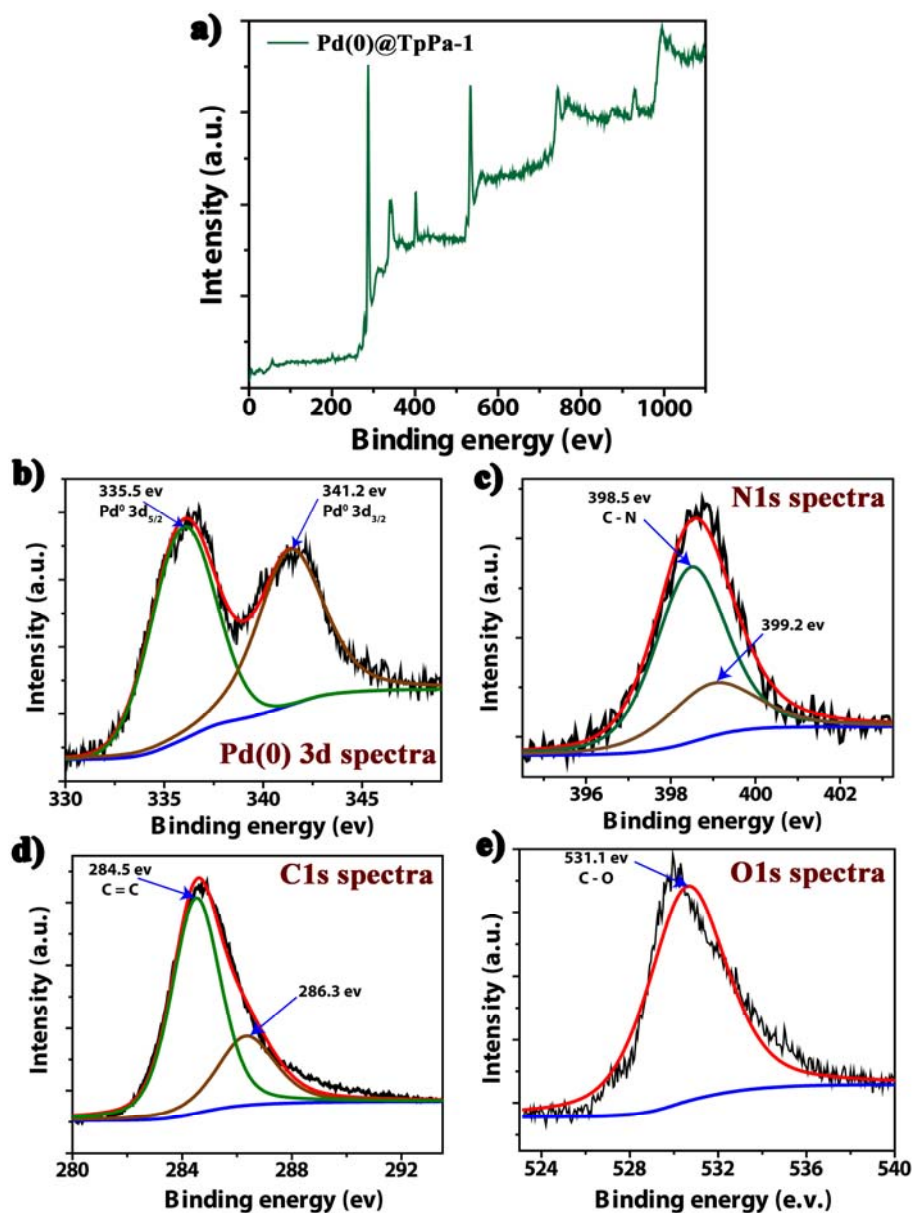


Figure S8. XPS analysis of Pd(0)@TpPa-1 samples. a) Survey scan of Pd(0)@TpPa-1 samples showing overall spectra of Pd, N, C and O atoms. b) XPS spectrum of the Pd(0)@TpPa-1 in the Pd3d region showing characteristic peaks at 335.5 eV ($\text{Pd}^0 3d_{5/2}$) and 341.2 eV ($\text{Pd}^0 3d_{3/2}$) for Pd(0). c) N1s spectra showing characteristic peaks at 398.5 eV for C–N stretching of TpPa-1 and 399.2 eV for other –N atoms (probably Pd...N) in Pd(0)@TpPa-1. d) C1s spectra showing characteristic peaks at 284.5 eV for C=C stretching of TpPa-1 and 286.3 eV for other –C atoms in Pd(0)@TpPa-1. e) O1s spectra showing characteristic peak at 531.1 eV for C–O stretching of TpPa-1.

Section S4. Synthesis and characterization of Pd(II)@TpPa-1

Synthesis of **Pd(II)@TpPa-1** was performed using palladium (II) acetate [Pd(OCOCH₃)₂] as a metal precursor. Activated **TpPa-1** (100 mg) was impregnated with Pd(OCOCH₃)₂ (20 mg, 0.093 mmol). The mixture was subjected to sonication in ultrasonic bath for 30 min and subsequently stirred vigorously for 1 h at RT. The residue was filtered and washed several times (×3) using fresh aliquots of CH₃OH to yield **Pd(II)@TpPa-1**. The prepared sample of **Pd(II)@TpPa-1** was further dried in a vacuum drying oven at 50 °C.

IR (powder, cm⁻¹): 1584 (s), 1570 (w), 1446 (s), 1257 (s), 993 (s), 829 (s), 699 (w)

Elemental analysis. For **Pd(II)@TpPa-1**

Calculated: **C**, 59.1; **H**, 2.94; **N**, 11.78

Found: **C**, 58.51; **H**, 2.85; **N**, 11.05

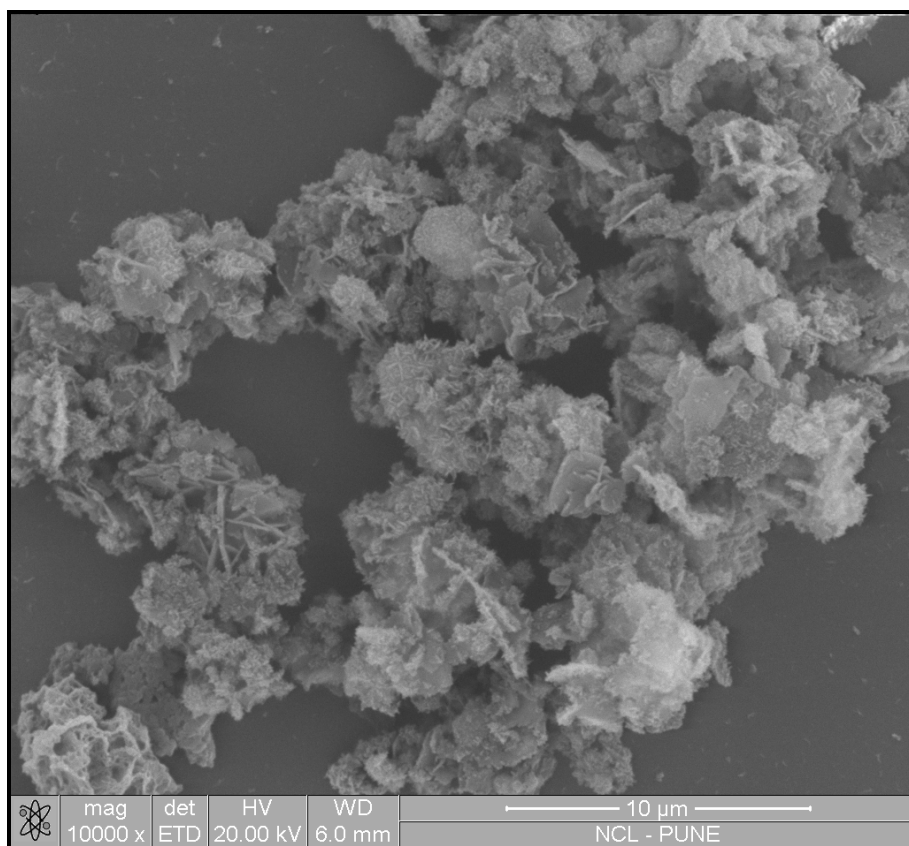


Figure S9. SEM image of the **Pd(II)@TpPa-1** showing the morphology of the **TpPa-1** after palladium (II) acetate loading. The maintained morphology of **Pd(II)@TpPa-1** with pristine **TpPa-1** shows the loading of Pd(II) into **TpPa-1** matrix without disturbing the COF morphology.

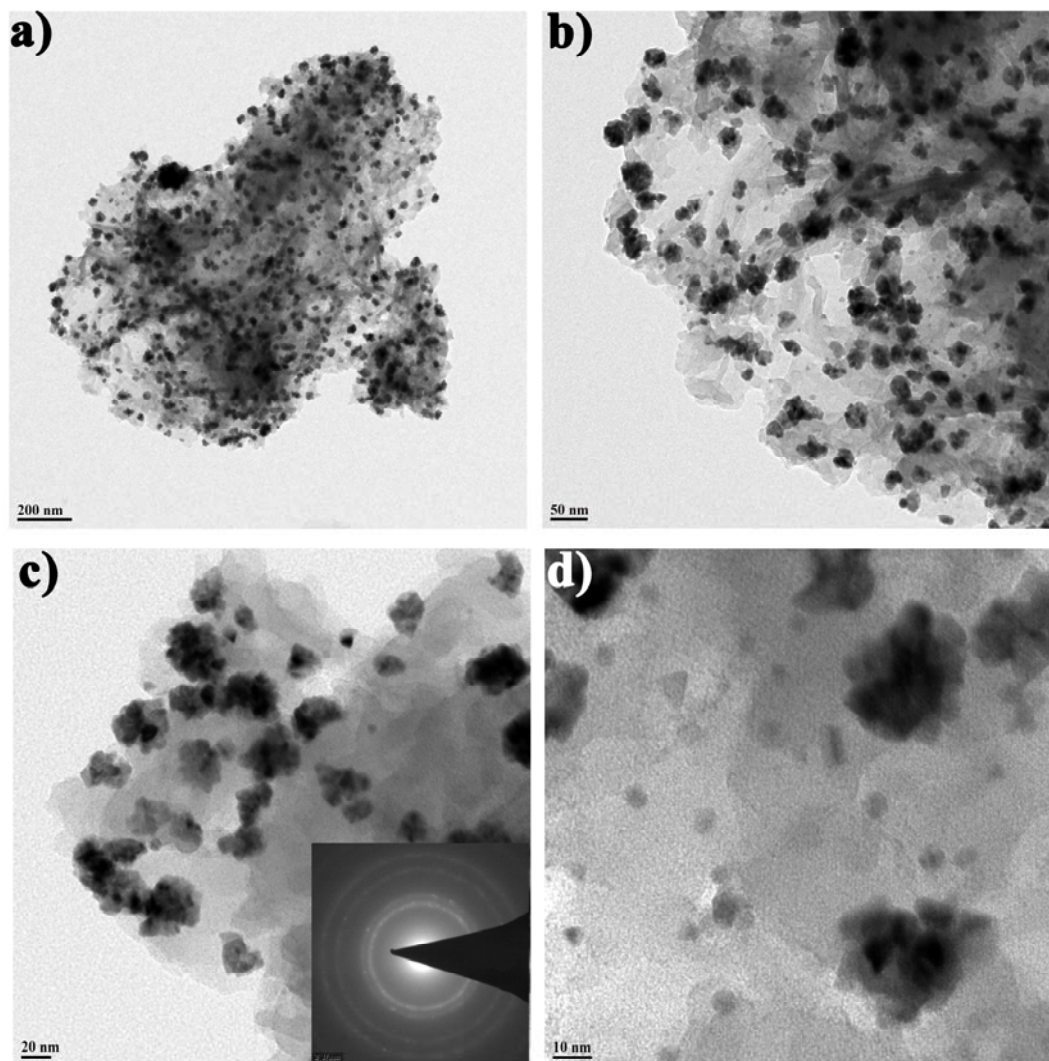


Figure S10. TEM images of **Pd(II)@TpPa-1**. a) Low resolution TEM image showing clusters of Pd distributed overall surface of **TpPa-1**. b) and c) Nanoclusters of 25 ± 10 nm size decorated on the layered structure of **TpPa-1**. Inset figure shows the SAED pattern of **Pd(II)@TpPa-1**. d) High resolution TEM image of Pd nanoclusters distributed on **TpPa-1** showing agglomerated Pd(0) particles.³ The jagged or rough nature of the Pd(0) nanoclusters in **Pd(II)@TpPa-1** than that of **Pd(0)@TpPa-1** observed in TEM analysis confirms that the loaded metals first gets agglomerated and further reduced during TEM analyses.

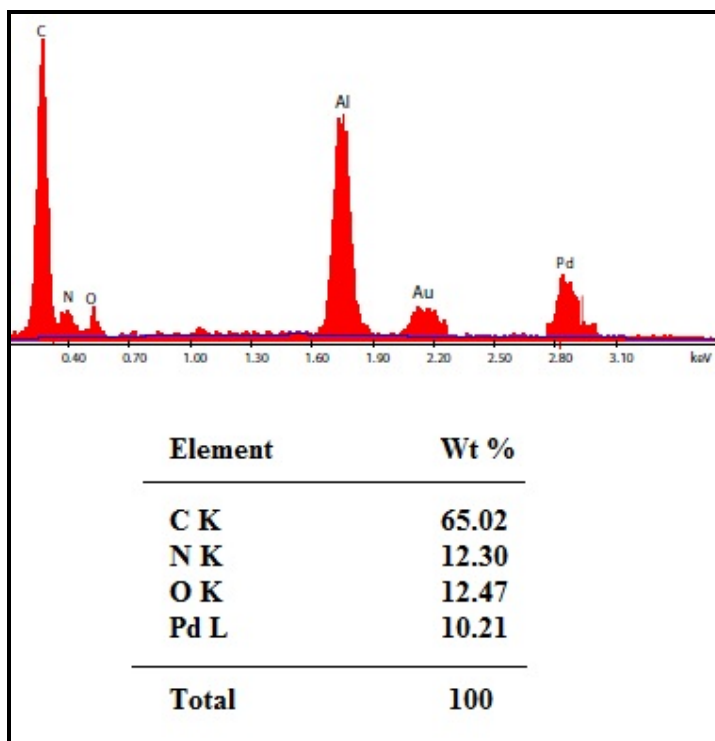


Figure S11. EDAX analysis of **Pd(II)@TpPa-1** showing 10.21 wt.% loading of Pd(II) into the **TpPa-1** matrix. The sample irradiated with high energy beam while performing TEM analyses was used for performing the EDX analyses.

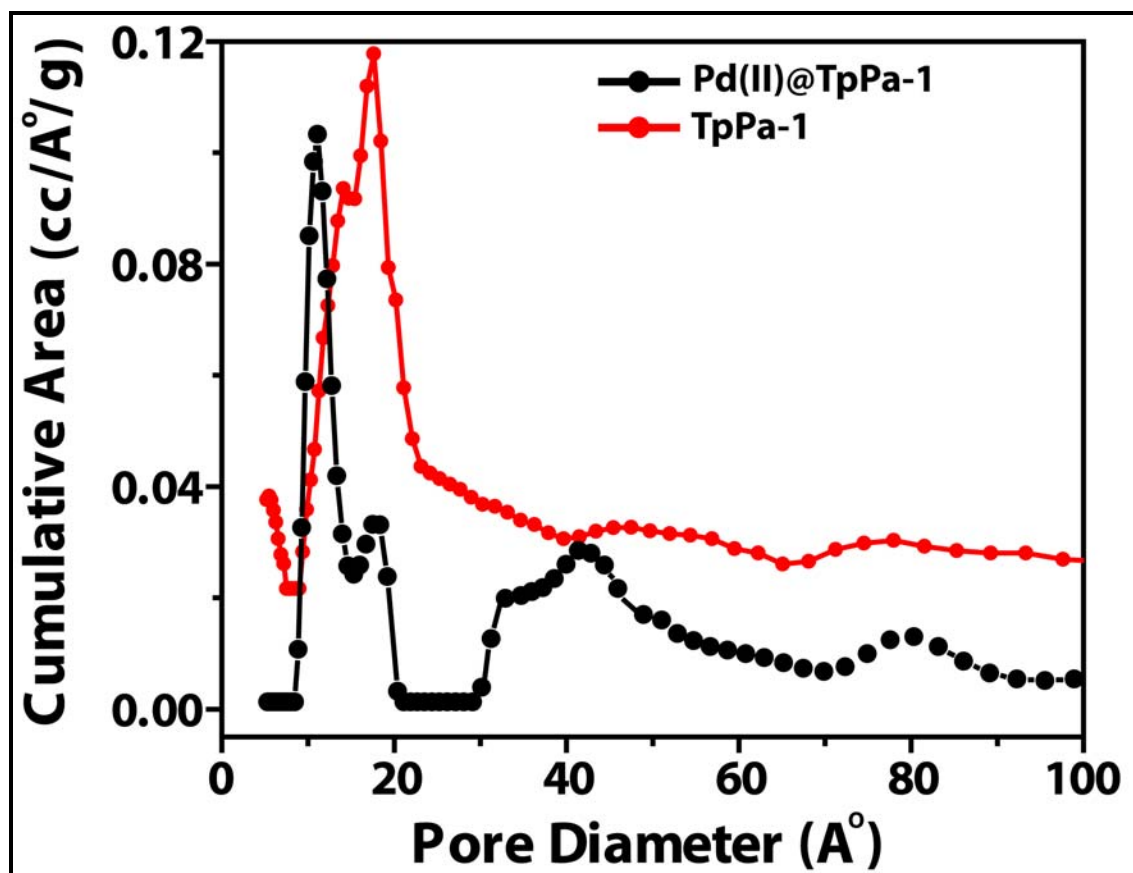


Figure S12. Pore size distribution analyses of Pd(II)@TpPa-1 and TpPa-1. DFT pore size distribution plots for TpPa-1 and Pd(II)@TpPa-1 show decrease in the pore size after Pd loading.

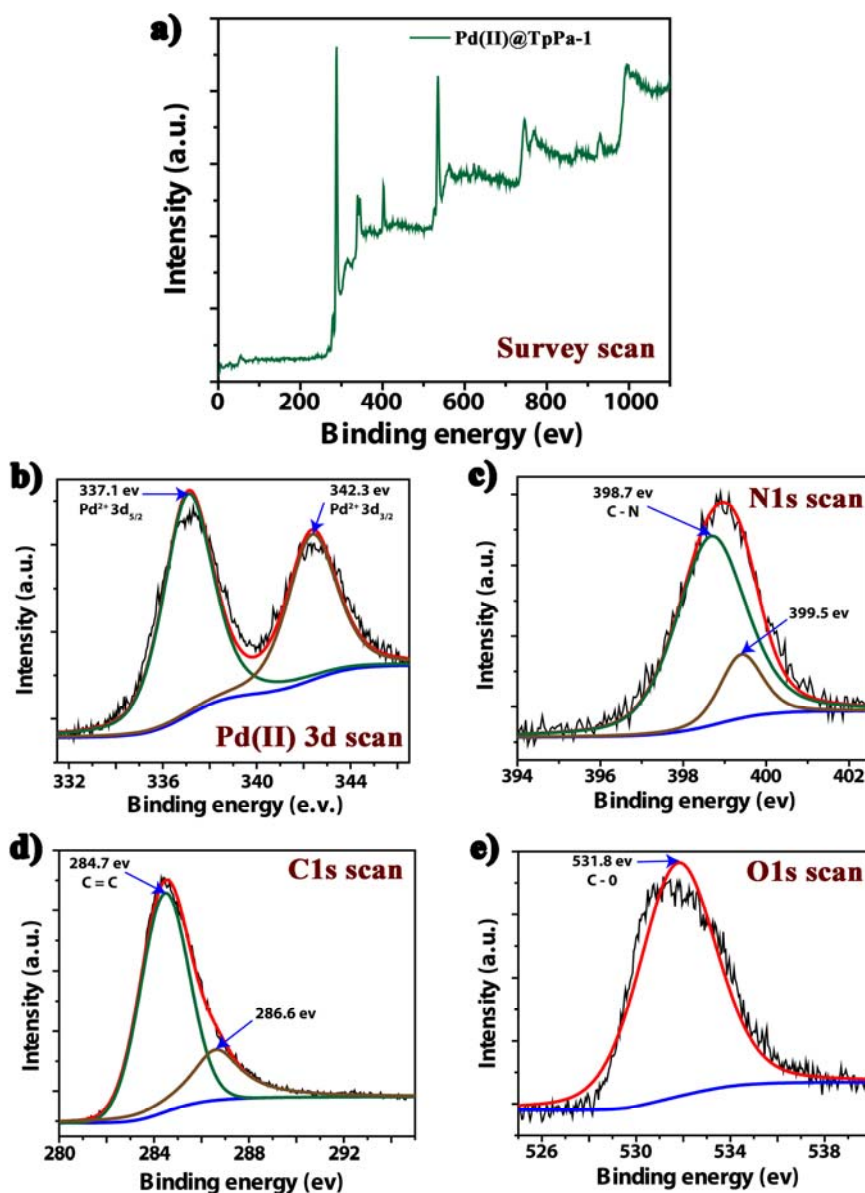


Figure S13. XPS analysis of **Pd(II)@TpPa-1** samples. a) Survey scan of **Pd(II)@TpPa-1** samples showing overall spectra of Pd, N, C and O atoms. b) XPS spectrum of the **Pd(II)@TpPa-1** in the Pd3d region showing characteristic peaks at 337.1 eV (Pd²⁺ 3d_{5/2}) and 342.3 eV (Pd²⁺ 3d_{3/2}) for Pd(II). c) N1s spectra showing characteristic peaks at 398.7 eV for C-N stretching of **TpPa-1** and 399.5 eV for other -N atoms (probably Pd acetate...N interaction) in **Pd(II)@TpPa-1**. d) C1s spectra showing characteristic peaks at 284.7 eV for C=C stretching of **TpPa-1** and 286.6 eV for other C atoms in **Pd(II)@TpPa-1**. e) O1s spectra showing characteristic peak at 531.8 eV for C-O stretching of **COF**.

Section S5. General procedures followed for catalytic reactions

General procedure for the Sonogashira coupling reaction:

In a typical reaction, a two neck round bottom flask was charged with aryl iodide (3.0 mmol), aliphatic/aromatic alkynes (3.3 mmol) and K_2CO_3 (829 mg, 6 mmol) in dry MeOH (10 mL). Nitrogen gas was bubbled through the solution for 30 min prior addition of Pd(0)@TpPa-1 (15 mg, 9.62×10^{-3} mmol of Pd). The reaction mixture was stirred at 105 °C for 6 h. After stipulated time; the reaction mixture was cooled to RT and filtered. The residue was extracted with CH_2Cl_2 (3×25 mL) and the combined organic layers were washed with water, dried over anhydrous Na_2SO_4 and analyzed by GC using decane (0.5 ml 2.0 % in methanol) as internal standard. In some cases, the compounds isolated after solvent evaporation were further purified by re-crystallization from suitable solvent. The desired coupling products were fully characterized by 1H NMR, ^{13}C NMR, melting point determination and single crystal X-ray crystallography (ESI, Section S7).

General procedure for the Heck coupling reaction:

In a typical run, a two neck round bottom flask was charged with a suitable aryl iodide (3.0 mmol), aliphatic/aromatic olefin (3.3 mmol) and K_2CO_3 (6 mmol) in 10 mL of MeOH. Nitrogen gas was purged through the solution for 20 min before the addition of catalyst Pd(0)@TpPa-1 (15 mg, 9.62×10^{-3} mmol of Pd). The reaction mixture was refluxed at 105 °C for 6 h atmosphere. After the specific reaction time, the mixture was cooled to RT and filtered. The product was extracted by CH_2Cl_2 (3×25 mL) and the organic layer was washed with water, dried over anhydrous Na_2SO_4 and analyzed by GC using decane (0.5 ml 2.0 % in methanol) as internal standard. The desired products were thoroughly characterized by 1H NMR, ^{13}C NMR, melting point determination and single crystal X-ray crystallography (ESI, Section S8).

Sequential one pot Heck/Sonogashira coupling reactions:

In a round bottom flask, 5 mL DMF, 4-Bromiodobenzene (283 mg, 1.0 mmol), tert-butyl acrylate/styrene (1.05 mmol), NaOAc (100 mg, 1.2 mmol) and Pd(0)@TpPa-1 (20 mg, 1.28×10^{-2} mmol of Pd) were added. The solution was heated to 120 °C for 2 h. The mixture was then allowed to cool to room temperature and phenylacetylene (153 mg, 1.5 mmol), Cs₂CO₃ (400 mg, 1.2 mmol), CuI (3 mg, 1.5 mol %) and PPh₃ (3 mg, 1.0 mol %) were added to the same reaction pot and heated to 105 °C for another 4 h. The product was extracted by CH₂Cl₂ (3 × 25 mL) and the organic layer was washed with water, dried over anhydrous Na₂SO₄. The organic phase was analyzed by GC using decane (0.5 ml 2.0 % in methanol) as internal standard. The desired purified products were thoroughly characterized by ¹H NMR, ¹³C NMR (ESI, Section S9).

General procedure for the intramolecular oxidative biaryl synthesis:

In a typical reaction, a round bottom flask was charged with diphenylamine (84.6 mg, 0.5 mmol), K₂CO₃ (6.9 mg, 0.05 mmol) and 30 mg of the catalyst Pd(II)@TpPa-1 (1.92×10^{-2} mmol) was heated to reflux in acetic acid or pivalic acid (450 mg) at 120 °C under air for 12 h. After this time, the reaction mixture was cooled to RT and the mixture extracted with CH₂Cl₂ (3 × 25 mL). The combined organic layers were washed repeatedly with saturated Na₂CO₃ solution, dried over anhydrous Na₂SO₄ and the solvent evaporated to dryness under reduced pressure to obtain the desired product. The products were characterized by ¹H NMR and ¹³C NMR spectroscopy (ESI, Section S9).

Section S6. Optimization of reaction conditions

1. Optimization of base:

Table S1. Sonogashira coupling between iodobenzene and phenylacetylene in the presence of different bases.



Entry	Base	Time (h)	Conv. ^a (%)	Yield ^b (%)
1	No Base	6	02	-
2	K ₂ CO ₃	6	98	90
3	K ₃ PO ₄	6	94	86
4	KOH	6	95	89
5	NH ₄ OH	6	74	70
6 ^c	Et ₃ N	6	92	88

^a Reactant conversion calculated using GC analysis.

^b Isolated yield.

^c Temperature here was set to 90 °C to avoid evaporation of Et₃N.

2. Optimization of solvent

Table S2. Sonogashira coupling between iodobenzene and phenylacetylene in different solvents.



Entry	Solvent	Time (h)	Temp (°C)	Conv. ^a (%)	Yield ^b (%)
1	CH ₃ OH	6	105	98	90
2	CH ₃ CN	8	115	65	56
3	Toluene	9	125	45	40
4	iPrOH	7	110	78	71
5	H ₂ O:iPrOH (1:1 v/v)	7	110	49	42
6	H ₂ O	9	110	02	-
7	H ₂ O:CH ₃ OH (1:9 v/v)	6	105	92	87
8	H ₂ O:CH ₃ OH (1:4 v/v)	6	105	75	71
9	H ₂ O:CH ₃ OH (1:1 v/v)	6	110	58	50
10	H ₂ O:CH ₃ OH (4:1 v/v)	6	110	46	43
11.	H ₂ O:CH ₃ OH (9:1 v/v)	6	110	31	25

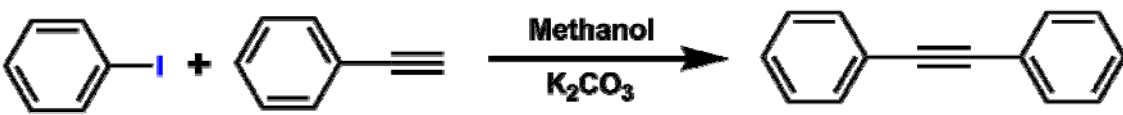
^a Reactant conversion calculated using GC analysis.

^b Isolated yield.

^c Temperature here was set to 90 °C to avoid evaporation of Et₃N.

3. Optimization of temperature, time, catalyst loading

Table S3. Optimization of reaction conditions for the Sonogashira coupling between iodobenzene and phenylacetylene.



Entry	Temperature (°C)	Time (h)	Catalyst loading (mg) ^a	Conv. ^b (%)	Yield ^c (%)
1.	105	6	15	98	90
2.	90	6	15	77	71
3.	105	2	15	32	25
4.	105	4	15	69	62
5.	105	5	15	81	74
6.	105	6	15	98	90
7.	105	6	5	41	34
8.	105	6	10	67	59
9.	105	6	15	97	86
10. ^d	105	6	15 mg COF TpPa-1	2	-
11. ^e	105	6	No catalyst	2	-

^a Unless otherwise noted, the catalyst used was **Pd(0)@TpPa-1**.

^b Reactant conversion calculated using GC analysis.

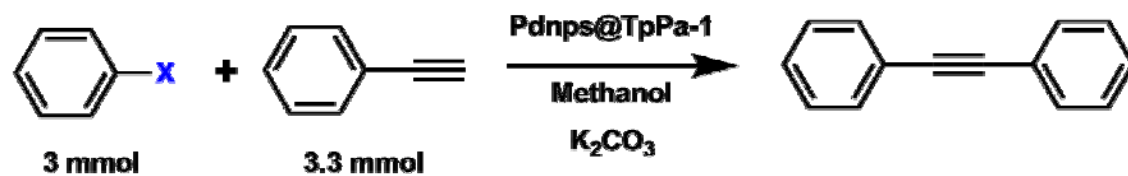
^c Isolated yield.

^d In this case, COF (**TpPa-1**) was used to check its inertness towards Sonogashira reaction.

^e Aforementioned reaction was performed without any catalyst.

4. Optimization of Aryl Halide

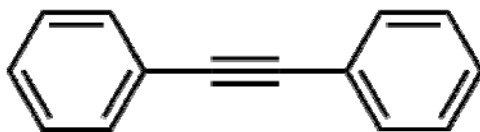
Table S4. Optimization of aryl halide for the Sonogashira coupling reaction with phenylacetylene.



Entry	X	Time (h)	Temp (°C)	Conv. ^a (%)	Yield ^b (%)
1	- I	6	105	98	90
2	- Br	> 9	105	68	62
3	- Cl	> 9	105	29	23

Section S7. Product characterization of Sonogashira coupling reactions:

1,2-Diphenylethyne (Table 1, Entry 1 and 9)



White solid, 92 % yield

Melting point: 54-55 °C

^1H NMR (CDCl_3 , 200 MHz): δ 7.55-7.53 (m, 4H), 7.37-7.34 (m, 6H).

^{13}C NMR (CDCl_3 , 50 MHz): δ 131.5, 128.3, 127.9, 122.9, 89.3

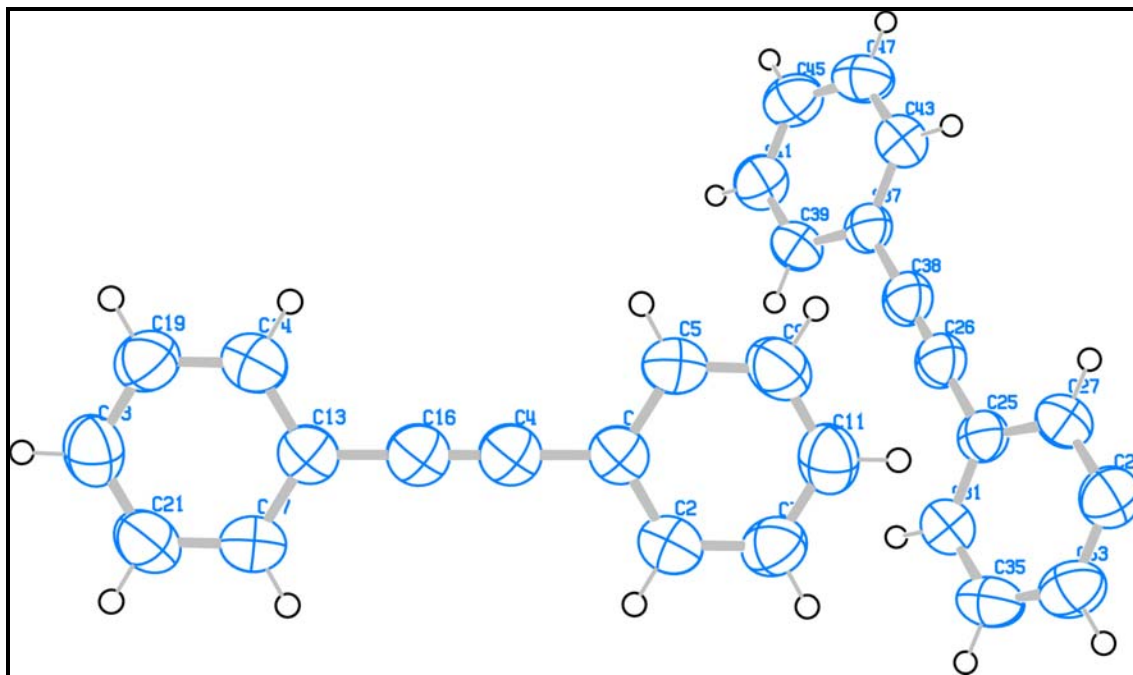
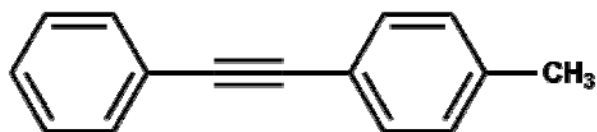


Figure S14. ORTEP diagram of 1,2-diphenylethyne (1,2-dpe) crystallized by slow evaporation of CH_3OH .

1-Methyl-4-(phenylethynyl)benzene (Table 1, Entry 2)



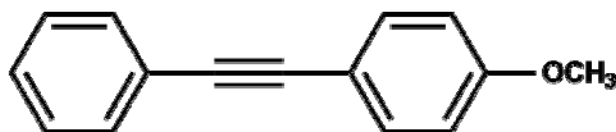
White solid, 89 % yield

Melting point: 69-70 °C

¹H NMR (CDCl₃, 200 MHz): δ 7.54-7.41 (m, 2H), 7.46-7.42 (m, 2H), 7.36-7.34 (m, 3H), 7.19- 7.15 (m, 2H), 2.38 (s, 3H)

¹³C NMR (CDCl₃, 50 MHz): δ 137.7, 131.5, 129.1, 128.3, 118.0, 88.7, 21.5

1-methoxy-4-(phenylethynyl)benzene (Table 1, Entry 3)



Pale yellow solid, 78 % yield

Melting point: 59-60 °C

¹H NMR (CDCl₃, 200 MHz): δ 7.55-7.53 (m, 4H), 7.36-7.33 (m, 3H), 6.89 (d, J = 7.2 Hz, 2H), 3.84 (s, 3H)

¹³C NMR (CDCl₃, 50 MHz): δ 160.2, 136.6, 132.0, 129.0, 128.9, 123.5, 116.3, 114.6, 90.1, 55.9

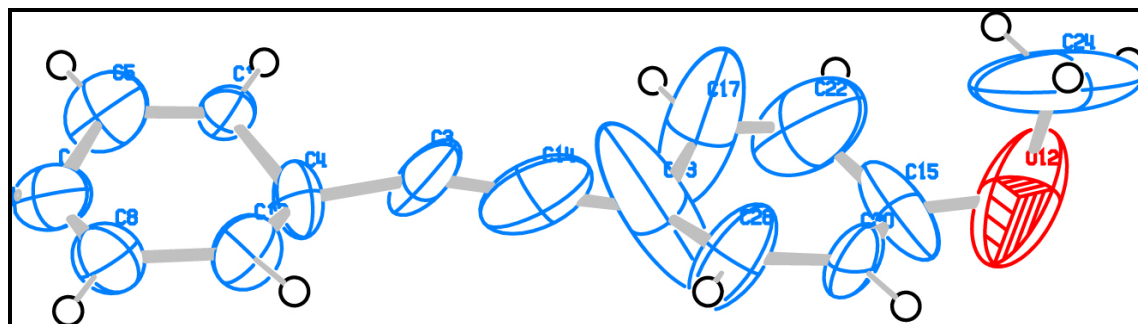
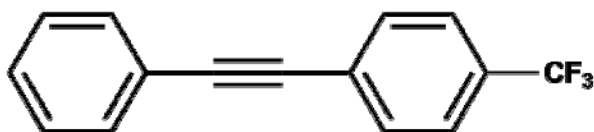


Figure S15. ORTEP diagram of 1-methoxy-4-(phenylethynyl)benzene crystallized by slow evaporation of CH₃OH solvent at RT.

1-(Phenylethynyl)-4-(trifluoromethoxy)benzene (Table 1, Entry 4)



White solid, 76 % yield

Melting point: 102-104 °C

¹H NMR (CDCl₃, 200 MHz): δ 7.68-7.63 (m, 4H), 7.55-7.52 (m, 2H), 7.40-7.37 (m, 3H)

¹³C NMR (CDCl₃, 50 MHz): δ 131.7, 131.4, 128.8, 128.4, 125.2, 124.9, 124.7, 89.0

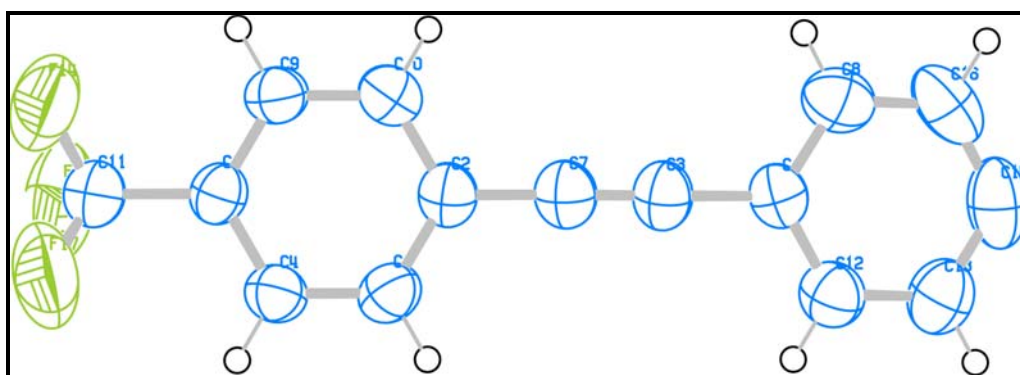
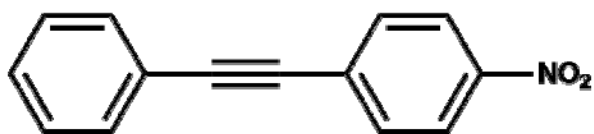


Figure S16. ORTEP diagram of 1-(phenylethynyl)-4-(trifluoromethoxy)benzene crystallized by slow evaporation of CH₃OH solvent at RT.

1-Nitro-4-(phenylethynyl)benzene (Table 1, Entry 5)



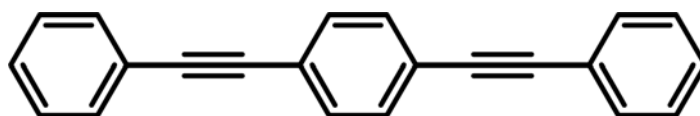
Yellow solid, 74 % yield

Melting point: 120-121 °C

¹H NMR (CDCl₃, 200 MHz): δ 8.27-8.21 (m, 2H), 7.71-7.66 (m, 2H), 7.57-7.52 (m, 2H), 7.42-7.39 (m, 3H)

¹³C NMR (CDCl₃, 50 MHz): δ 146.9, 132.2, 1321.8, 130.2, 129.2, 128.6, 123.6, 122.0, 94.6, 87.5

1,4-Bis(phenylethynyl)benzene (Table 1, Entry 6)



White solid, 86 % yield

Melting point: 176-178 °C

^1H NMR (CDCl_3 , 200 MHz): δ 8.57-8.52 (m, 8H), 7.38-7.36 (m, 6H)

^{13}C NMR (CDCl_3 , 50 MHz): δ 131.5, 131.3, 128.3, 127.8, 123.0, 89.0

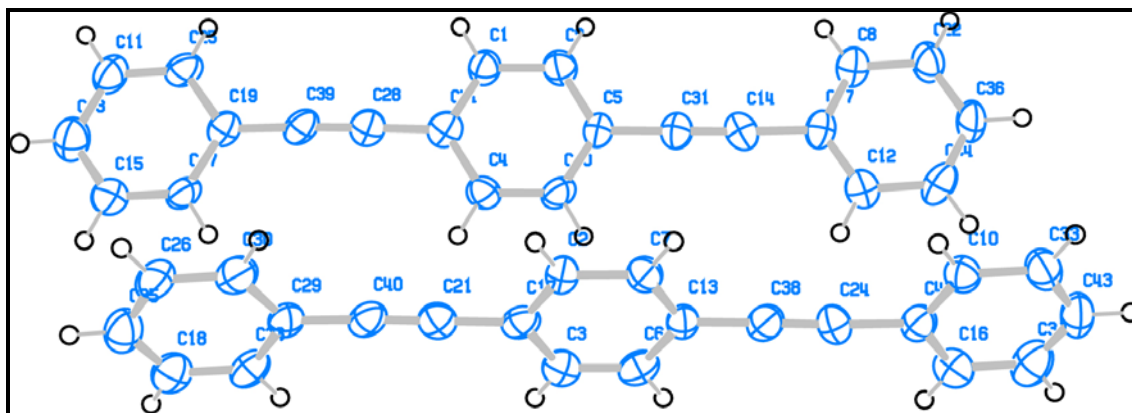
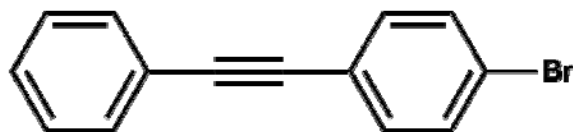


Figure S17. ORTEP diagram of 1,4-bis(phenylethynyl)benzene crystallized by slow evaporation of CH_3OH solvent at RT.

1-Bromo-4-(phenylethynyl)benzene (Table 1, Entry 7)



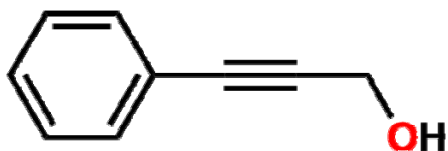
Pale yellow solid, 60 % yield

Melting point: 104-106 °C

^1H NMR (CDCl_3 , 200MHz): δ 7.62-7.58 (m, 4H), 7.44-7.40 (m, 3H), 7.18-7.15 (m, 2H)

^{13}C NMR (CDCl_3 , 50 MHz): δ 135.4, 133.6, 132.8, 129.2, 127.9, 123.1, 122.6, 89.1

3-Phenylprop-2-yn-1-ol (Table 1, Entry 10)



Yellow liquid, 94 % yield

Boiling point: 128-130 °C

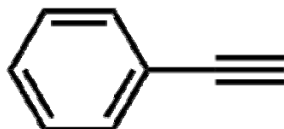
¹H NMR (CDCl₃, 200MHz): δ 4.34 (s, 2H), 7.28 (m, 3H), 7.37 (m, 2H)

¹³C NMR (CDCl₃, 50 MHz): δ 127.5, 121.3, 99.8, 87.5, 49.7

Trimethyl(phenylethynyl)silane (Table 1, Entry 11)



As we have used excess base (K₂CO₃) in methanol for this reaction, desilynation of the above product took place and resulted into the formation phenylacetylene.⁴



Yellow liquid, 92 % yield

Boiling point: 142-144 °C

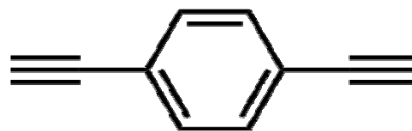
¹H NMR (CDCl₃, 200MHz): δ 7.55-7.48 (m, 2H), 7.42-7.35 (m, 2H), 3.02 (s, 1H)

¹³C NMR (CDCl₃, 50 MHz): δ 133.1, 128.9, 123.0, 85.6, 77.9

1,4-bis(trimethylsilyl)ethynylbenzene (Table 1, Entry 12)



As we have used excess base (K₂CO₃) in methanol for this reaction, desilynation of the above product took place and resulted into the formation 1,4-diethynylbenzene.⁴



Yellowish powder, 90 % yield

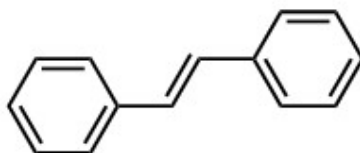
Melting point: 95-97 °C

^1H NMR (CDCl_3 , 200MHz): δ 7.38-7.25 (m, 4H), 2.14 (s, 2H)

^{13}C NMR (CDCl_3 , 50 MHz): δ 133.5, 123.7, 85.6, 79.9

Section S8. Product characterization of Heck coupling reactions:

(*E*)-1,2-Diphenylethene (*trans*-Stilbene) (Table 2, Entry 1)



Off-white solid, 92 % yield

Melting point: 124 °C

^1H NMR (CDCl_3 , 200 MHz): δ 7.42-7.38 (m, 4H) 7.27-7.24 (m, 2H), 7.13-7.09 (m, 4H), 6.99 (s, 2H)

^{13}C NMR (CDCl_3 , 50 MHz): δ 138.2, 129.8, 128.8, 128.2

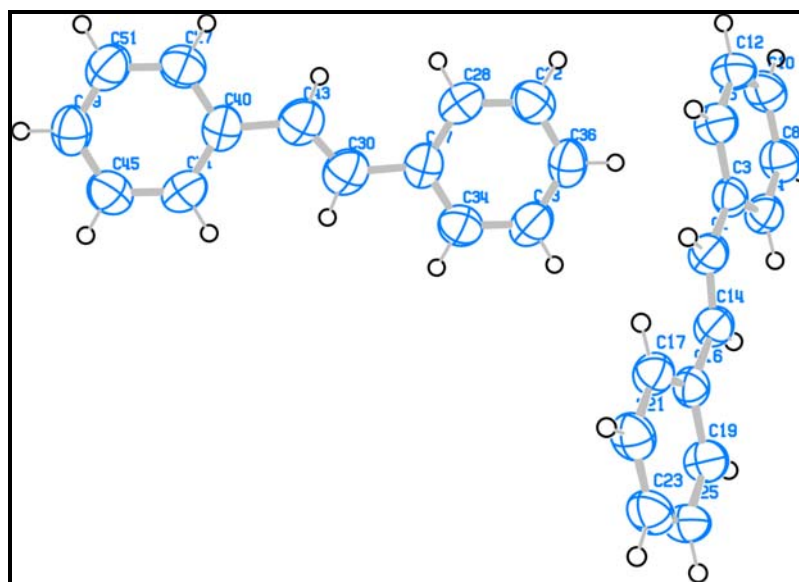
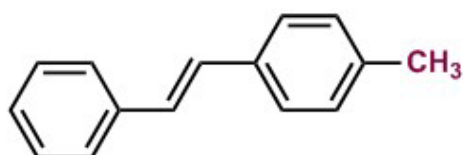


Figure S18. ORTEP diagram of (*E*)-1,2-diphenylethene crystallized by slow evaporation of CH_3OH solvent at RT.

(*E*)-1-Methyl-4-styrylbenzene (Table 2, Entry 2)



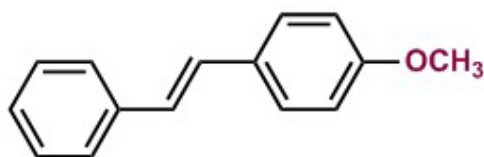
White solid, 88 % yield

Melting point: 116-119 °C

^1H NMR (CDCl_3 , 200 MHz): δ 7.52-7.46 (m, 4H) 7.14-7.11 (m, 4H), 7.03 (s, 1H), 6.88 (s, 2H), 2.29 (s, 3H)

^{13}C NMR (CDCl_3 , 50 MHz): δ 137.1, 134.2, 129.3, 128.7, 127.3, 126.4, 20.8

(E)-1-Methoxy-4-styrylbenzene (Table 2, Entry 3)



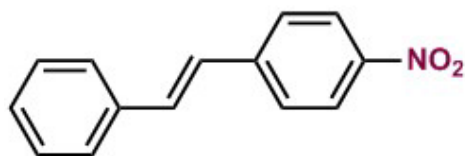
White solid, 80 % yield

Melting point: 130-132 °C

^1H NMR (CDCl_3 , 200 MHz): δ 7.58-7.51 (m, 4H) 7.32-7.29 (m, 2H), 7.23 (s, 1H), 7.14-7.10 (m, 2H), 7.02-6.99 (m, 2H), 3.75 (s, 3H)

^{13}C NMR (CDCl_3 , 50 MHz): δ 158.9, 137.3, 129.6, 128.6, 126.1, 114.2, 55.1

(E)-1-Nitro-4-styrylbenzene (Table 2, Entry 4)



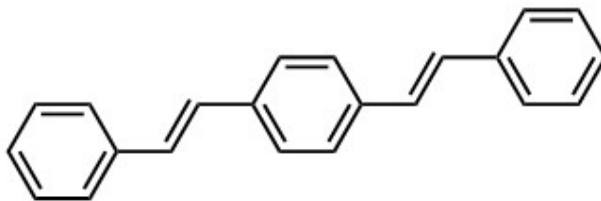
Yellowish solid, 77 % yield

Melting point: 155-157 °C

^1H NMR (CDCl_3 , 200 MHz): δ 8.35 (m, 2H), 7.71 (m, 2H), 7.62 (m, 2H), 7.45-7.55 (m, 3H), 7.30 (d, $J = 7.5$ Hz, 1H), 7.12 (d, $J = 7.3$ Hz, 1H)

^{13}C NMR (CDCl_3 , 50 MHz): δ 146.8, 149.9, 135.8, 133.0, 128.87, 127.82, 127.1, 126.5, 126.1, 123.4

1,4-Di((*E*)-styryl)benzene (Table 2, Entry 5)



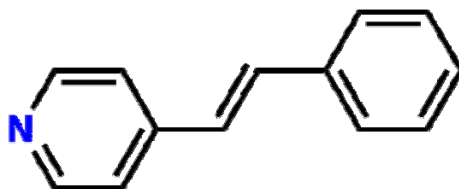
White solid, 85 % yield

Melting point: 215-217 °C

^1H NMR (CDCl_3 , 200 MHz): δ 7.63-7.59 (m, 4H), 7.39-7.35 (m, 8H), 7.26 (d, $J = 7.5$ Hz, 2H), 7.02 (s, 4H).

^{13}C NMR (CDCl_3 , 50 MHz): δ 137.5, 136.8, 129.5, 128.9, 128.7, 127.2.

(*E*)-4-Styrylpyridine (Table 2, Entry 6)



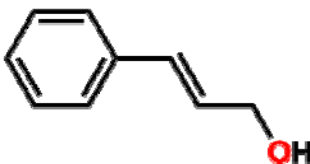
Yellow solid, 91 % yield

Melting point: 129-131 °C

^1H NMR (CDCl_3 , 200 MHz): δ 8.59 (s, br, 2H), 7.53-7.57 (m, 2H), 7.48-7.36 (m, 6H), 7.06-6.98 (d, $J = 7.2$ Hz, 2H)

^{13}C NMR (CDCl_3 , 50 MHz): δ 150.2, 144.6, 136.2, 128.9, 127.1, 126.0, 120.9

(*E*)-3-Phenylprop-2-en-1-ol (Table 2, Entry 7)



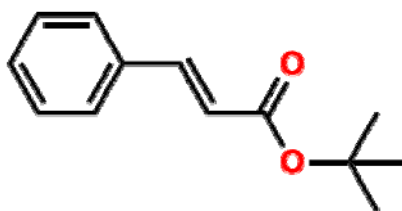
Yellow liquid, 91 % yield

Boiling point: 250-252 °C

^1H NMR (CDCl_3 , 200 MHz): δ 7.44–7.39 (m, 2H), 7.36–7.32 (m, 2H), 7.30–7.24 (m, 1H), 6.78 (d, $J = 10.2$ Hz, 1H), 6.44–6.39 (m, 1H), 4.32–4.31 (m, 2H), 1.65 (s, 1H)

^{13}C NMR (CDCl_3 , 50 MHz): δ 137.8, 132.3, 129.1, 128.8, 128.1, 127.1, 64.2

***tert*-Butyl cinnamate (Table 2, Entry 8)**



Colorless liquid, 93 % yield

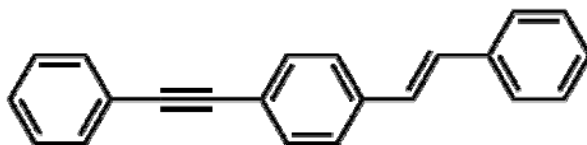
Boiling point: 83 °C

^1H NMR (CDCl_3 , 200 MHz): δ 7.60–7.55 (m, 3H), 7.42–7.37 (m, 3H), 6.44 (d, $J = 10.4$ Hz, 1H), 1.65 (s, 9H)

^{13}C NMR (CDCl_3 , 50 MHz): δ 166.5, 143.9, 135.1, 130.5, 129.7, 127.9, 121.7, 81.3, 28.5

Section S9. Product characterization of Sequential Heck/Sonogashira coupling reactions and intramolecular oxidative biaryl synthesis reactions:

(E)-1-(Phenylethynyl)-4-styrylbenzene (Table 3, Entry 1)

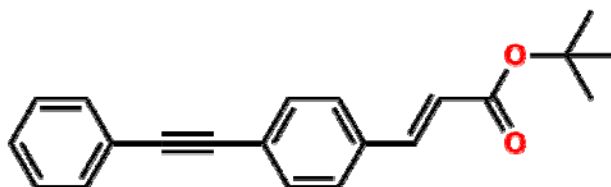


Colorless solid, 62 % yield

^1H NMR (CDCl_3 , 200 MHz): δ 7.49–7.41 (m, 8H), 7.28–7.20 (m, 5H), 6.32 (d, J = 11.1 Hz, 1H), 7.00–6.97 (m, 2H)

^{13}C NMR (CDCl_3 , 50 MHz): δ 138.8, 137.9, 132.5, 131.9, 130.2, 129.9, 128.8, 127.8, 127.5, 127.1, 126.8, 126.0, 122.9, 122.0, 89.7, 88.8

***tert*-Butyl (E)-3-(4-(phenylethynyl)phenyl)acrylate (Table 3, Entry 2)**

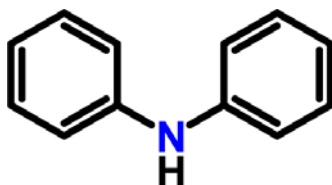


Yellow solid, 73 % yield

^1H NMR (CDCl_3 , 200 MHz): δ 7.54–7.43 (m, 6H), 7.31–7.28 (m, 4H), 6.32 (d, J = 10.3 Hz, 1H), 1.44 (s, 9H)

^{13}C NMR (CDCl_3 , 50 MHz): δ 167.2, 146.0, 136.2, 132.8, 128.9, 120.9, 117.9, 91.2, 83.8, 29.0

Diphenylamine



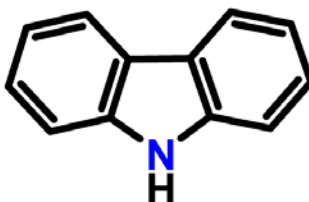
White colored crystalline solid

Melting point: 54 °C

^1H NMR (CDCl_3 , 200 MHz): δ 7.49-7.42 (m, 4H), 7.11-7.07 (m, 6H)

^{13}C NMR (CDCl_3 , 50 MHz): δ 142.1, 130.2, 122.7, 120.4

9H-carbazole



Beige colored crystalline solid

Melting point: 245-247 °C

^1H NMR (CDCl_3 , 200 MHz): δ 8.01-7.97 (m, 2H), 7.34-7.32 (m, 4H), 7.18-7.14 (m, 2H)

^{13}C NMR (CDCl_3 , 50 MHz): δ 140.2, 123.4, 121.9, 118.8, 111.2

Section S10. Catalyst leaching, recyclability and stability tests:

The following experiments were carried out in order to establish the stability of loaded Pd(0) nanoparticles on **TpPa-1**, and confirm the heterogeneous nature of the catalyst:

1. Pd leaching tests:

In a typical catalyst leaching test experiment, 15 mg of **Pd(0)@TpPa-1** catalyst and K_2CO_3 was taken in methanol and refluxed for 12 h and filtered in hot conditions into another round bottom flask. To this filtrate solution, required amount of the substrates (3.0 mmol iodobenzene, 3.3 mmol phenylacetylene) and K_2CO_3 was added and refluxed at 105 °C. The absence of the product after 12 h reaction confirmed the heterogeneous behaviour of the catalyst.

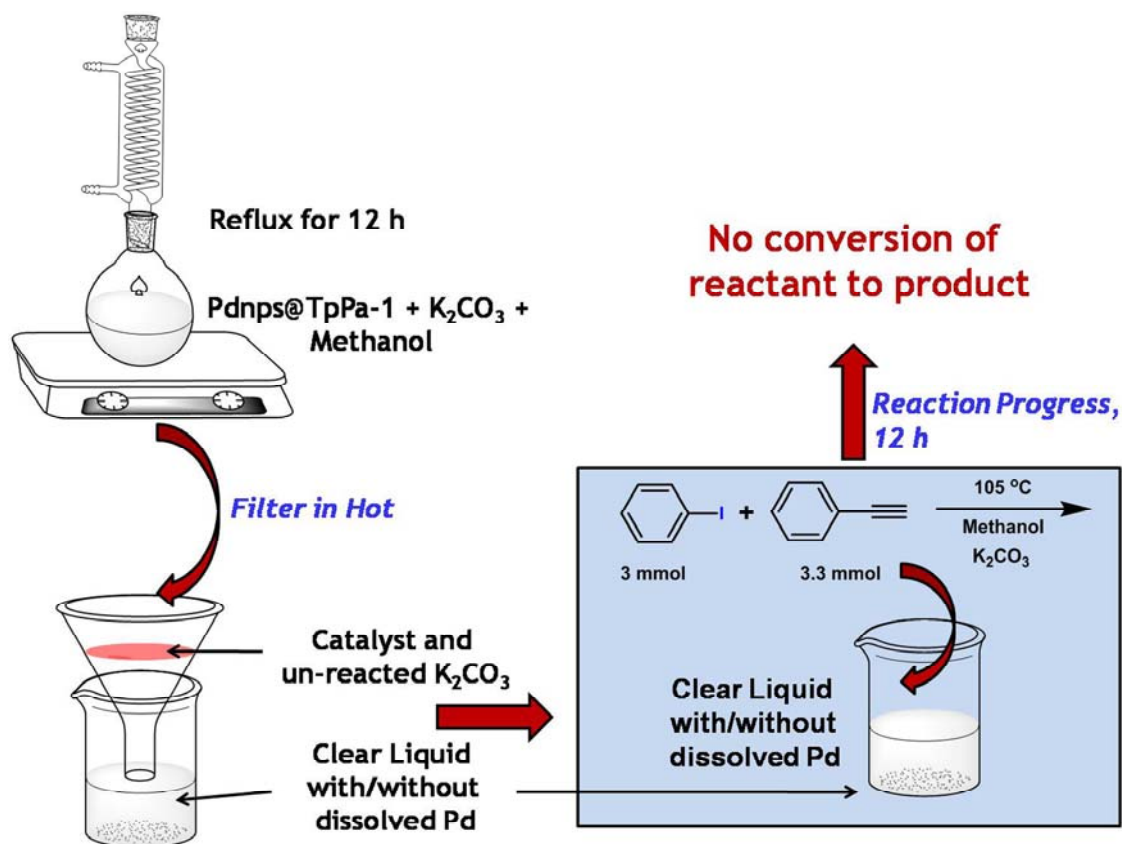


Figure S19. Pd catalyst leaching test performed for **Pd(0)@TpPa-1** catalyst by refluxing the catalyst in methanol for 12 h and then following the formation of 1,2-dpe by GC. The conversion of reactant in final step traced by GC analysis showed negligible conversion.

The EDX analysis of the clear solution obtained from above experiment after refluxing the **Pd(0)@TpPa-1** catalyst was performed to confirm the absence of Pd into the solution.

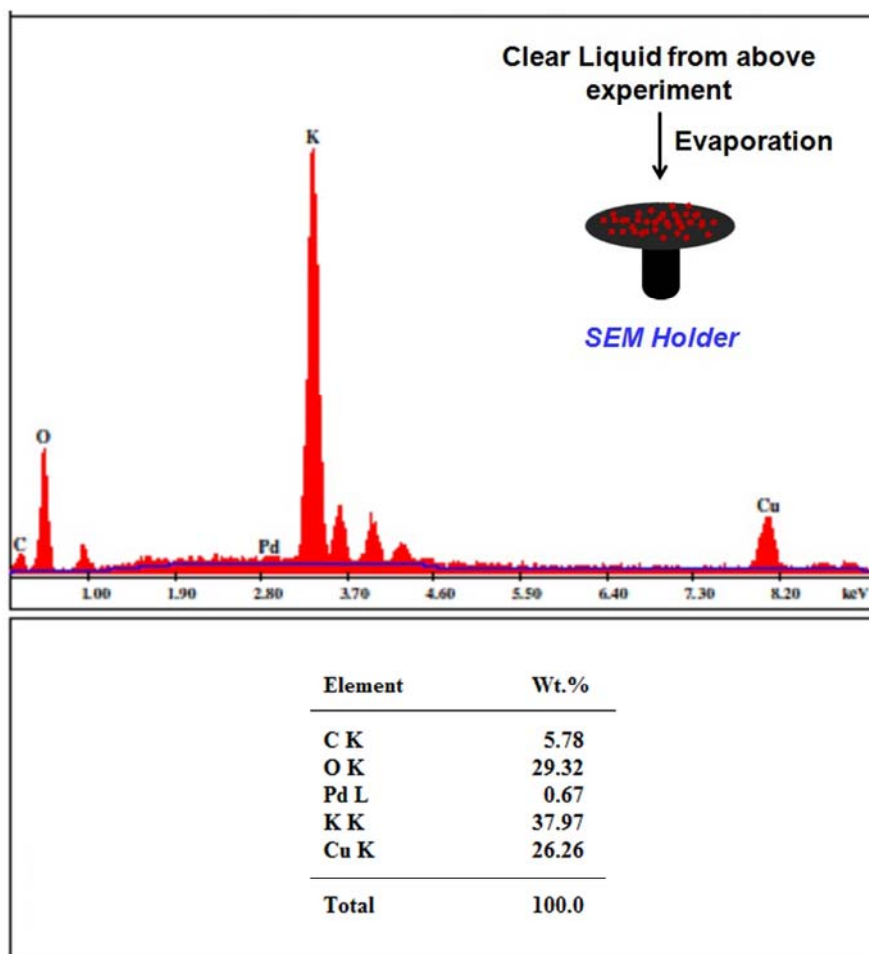


Figure S20. EDX analysis of the clear liquid showing almost negligible Pd content, which confirms the high stability of Pd(0) nanoparticles loading on **TpPa-1**. (High percentage of potassium present results from the excess of K_2CO_3 used).

2. Mercury drop test:

To establish the heterogeneity of the **Pd(0)@TpPa-1** catalyst in Sonogashira coupling reaction, we have carried out mercury drop experiment, in which the surface of the catalyst is poisoned and, in consequence, the catalytic activity reduced.

In a typical mercury drop test 3.0 mmol iodobenzene, 3.3 mmol phenylacetylene, K_2CO_3 and 15 mg of **Pd(0)@TpPa-1** catalyst was added. To this filtrate solution, a drop of mercury (50 mg) was added and the solution was refluxed at 105 °C for 12 h. The absence of the product after 12 h reaction confirmed the heterogeneous behaviour of the catalyst.

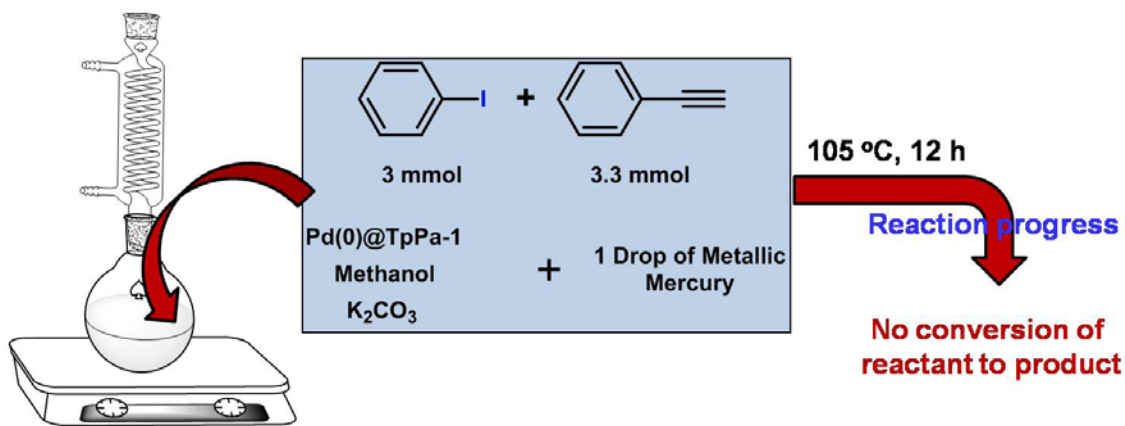
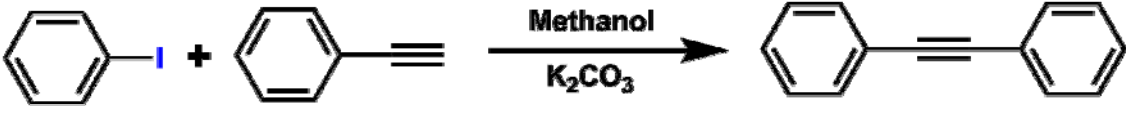


Figure S21. Mercury drop test performed for **Pd(0)@TpPa-1** catalyst. The conversion of reactant in product traced by GC analysis showed negligible conversion.

3. Catalyst recyclability experiments:

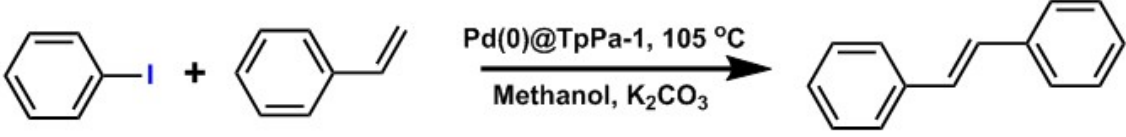
For the recyclability experiment, after each catalytic experiment, the catalyst from the reaction pot was isolated by filtration, washed thoroughly by methanol and used for the next cycle of experiment under same reaction condition.

Table S5. Recyclability of Pd(0)@TpPa-1 for Sonogashira coupling reaction:



Entry	Cycle No.	Conv. (%)	Yield (%)	TON	TOF (h ⁻¹)
1	1	98	90	305	51
2	2	87	81	271	46
3	3	78	72	243	41
4	4	72	65	224	37

Table S6. Recyclability of Pd(0)@TpPa-1 for Heck coupling reaction:



Entry	Cycle No.	Conv. (%)	Yield (%)	TON	TOF (h ⁻¹)
1	1	95	92	297	50
2	2	87	82	271	45
3	3	82	76	256	43
4	4	72	63	225	38

Recyclability of the model reaction in presence of water:

In order to check the recyclability of the catalyst **Pd(0)@TpPa-1**, the reaction done in the solvent system *Viz.* methanol: water = 9:1 and 1:1 mixtures. The results showed similar trends in the recyclability so as to 100 % methanol. The obtained results from this solvent system are assembled into the following figure.

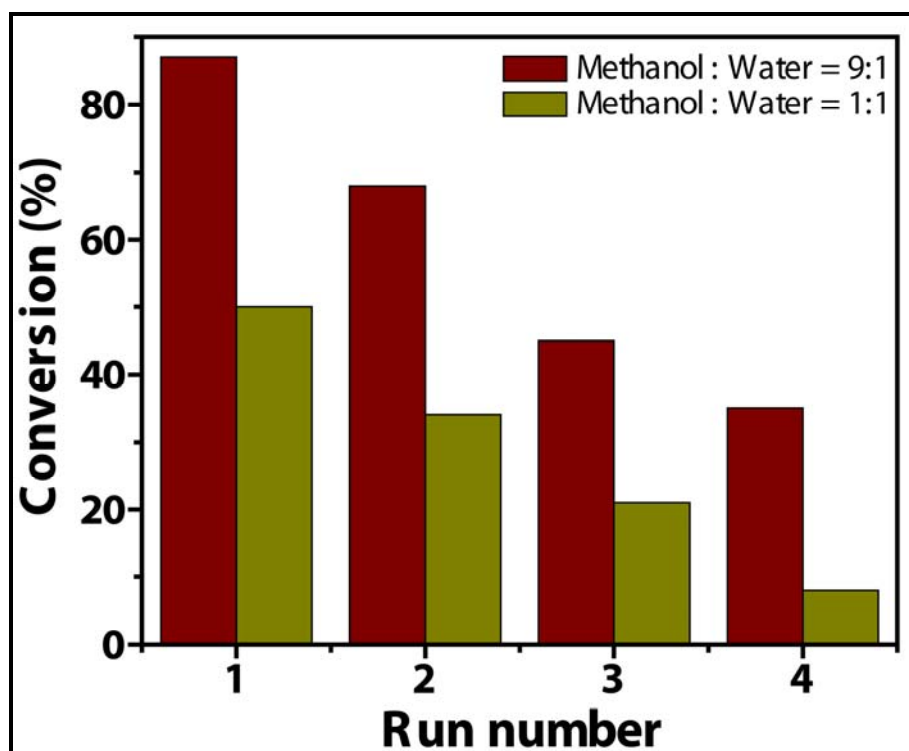


Figure S22. The recyclability of **Pd(0)@TpPa-1** catalyst for model reaction of 1,2-DPE synthesis performed in 9:1 and 1:1 methanol: water solvent system.

4. TEM analyses of reused COF and AC supported catalysts:

TEM images of the recovered catalyst were performed to confirm the catalyst stability. The stability of Pd(0)@TpPa-1 catalyst was compared with Pd(0)@AC catalyst. The presence of non-sintered and non-agglomerated Pd nanoparticles on TpPa-1 surface confirms the stability of these nanoparticles. The agglomeration of Pd nanoparticles decorated on AC demonstrates that the poor interaction between Pd nanoparticles and AC is not enough to hold these nanoparticles.

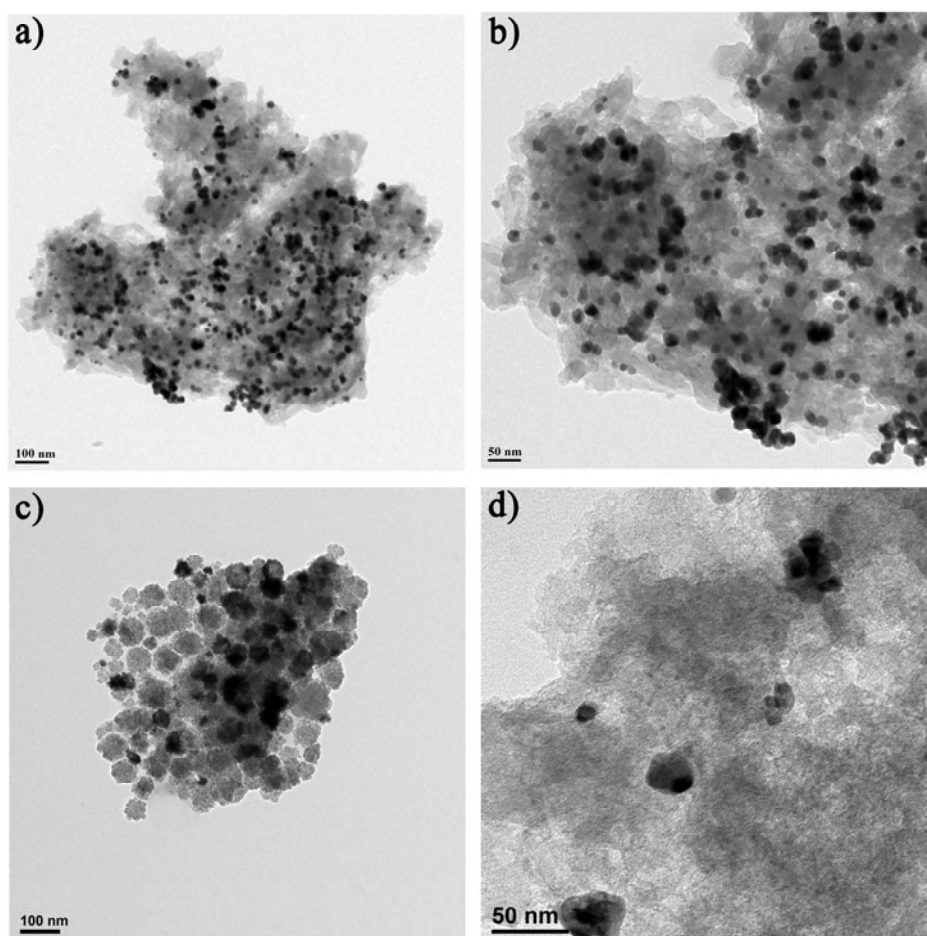


Figure S23. Comparative TEM images of reused Pd(0)@TpPa-1 and Pd(0)@AC catalyst. a-b) Distribution of Pd nanoparticles on the TpPa-1 surface after reaction for Pd(0)@TpPa-1, after 2nd cycle of the model reaction for 1,2-dpe synthesis. c-d) High resolution TEM image of the Pd(0)@AC catalyst after 1st cycle of the model reaction for 1,2-dpe synthesis, showing agglomerated nanoparticles.

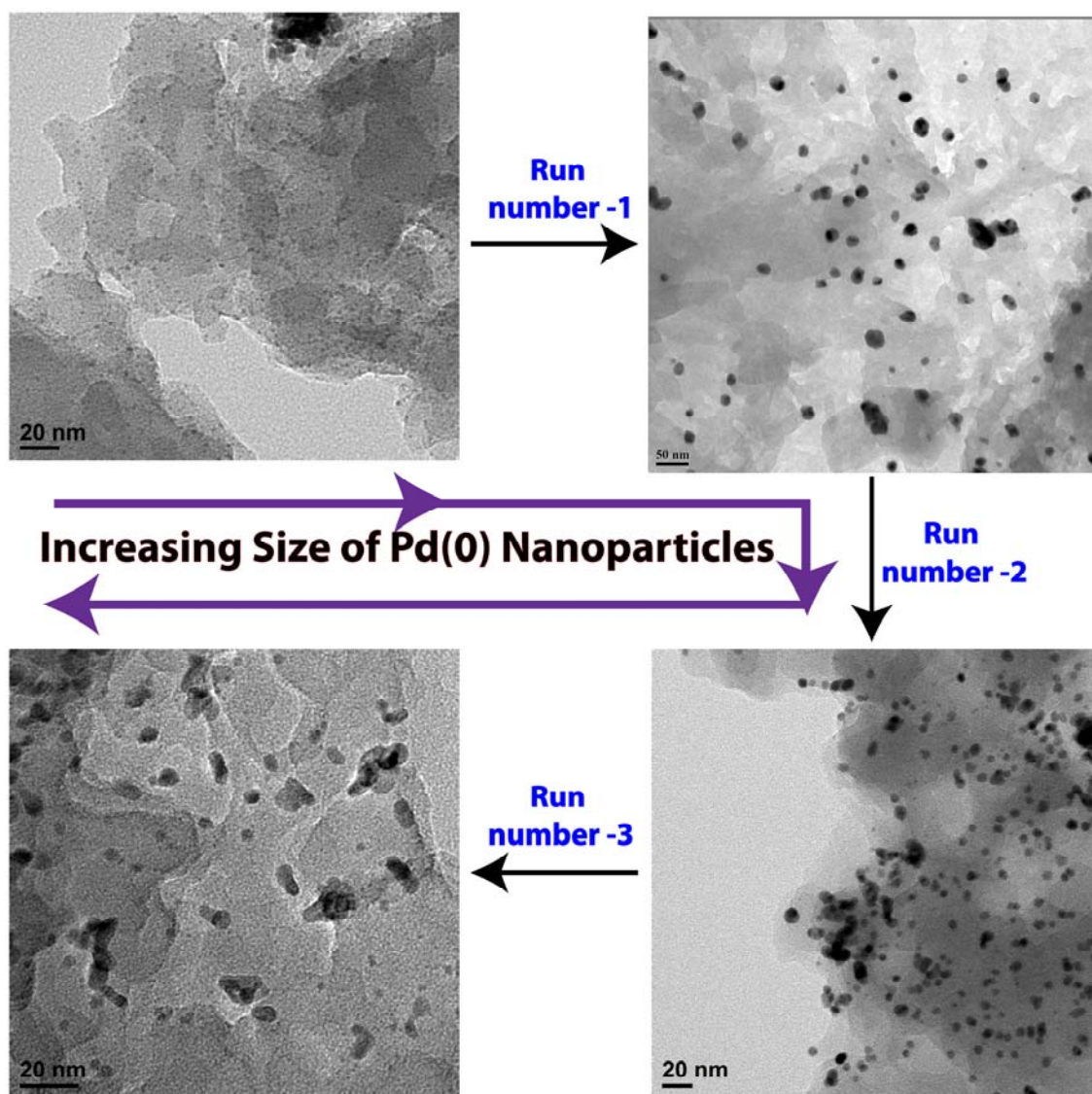
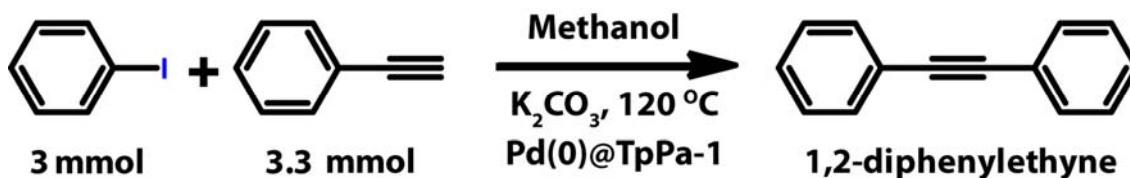


Figure S24. Change in the size of Pd(0) nanoparticles with increasing number of runs in **Pd(0)@TpPa-1**. The partial change in Pd(0) nanoparticle size was observed after 1st run. However, with increasing runs size of nanoparticles goes on increasing from 4 ± 2 nm to 10 ± 2 nm after 3rd run.

5. Carbon mass balance of the model reaction:

Regarding the catalyst **Pd(0)@TpPa-1** reported in this manuscript, we believe that the desorption of the small molecules, adsorbed during the course of the reaction, is facile as the support is two dimensional and has comparable pore size to the reactant and product molecules. In order to check the carbon mass balance of the reaction, we have performed the CHN analysis of the catalyst **Pd(0)@TpPa-1** before and after performing the following model reaction:



The results of the CHN analysis are as follows:

Pristine catalyst **Pd(0)@TpPa-1** before reaction:

Calculated: C, 64.77; H, 3.23; N, 12.92 (The elemental % is calculated considering 6.4 % loading of Pd(0) on **TpPa-1**, which is confirmed by using ICP/EDAX/TGA).

Found: C, 63.6; H, 3.12; N, 12.07

Catalyst **Pd(0)@TpPa-1** after reaction:

C, 64.11; H, 3.07; N, 13.45

From the aforementioned results, it is clear that the carbon percentage of the catalyst remains almost constant after the reaction. Hence, the likely adsorption of small molecules onto the 2D catalyst is followed by facile desorption.

6. Thermogravimetric analyses of Pd(0)@TpPa-1 and Pd(II)@TpPa-1:

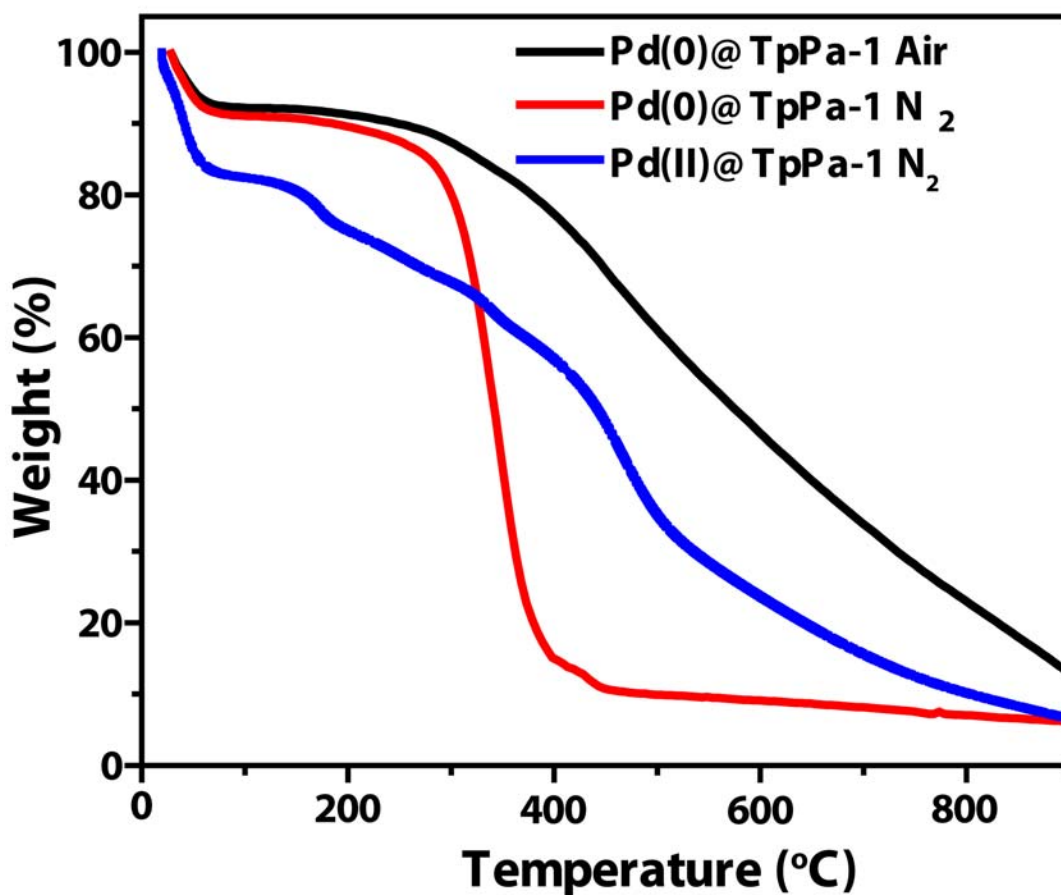


Figure S25. TGA profiles of Pd(0)@TpPa-1 and Pd(II)@TpPa-1 catalyst in N₂ and air atmosphere.

Table S7. Comparative changes in micropore surface area, pore size, total surface area and pore volume for the synthesized catalysts Pd(0)@TpPa-1 and Pd(II)@TpPa-1:

Sr. No.	Name of Sample	BET Surface Area (m ² /g)	Micropore Surface Area (m ² /g)	QSDFT Pore Volume (cc/g)	Average Pore Size (nm)
1	TpPa-1	484	242	0.546	1.78
2	Pd(0)@TpPa-1	226	87	0.269	1.60
3	Pd(II)@TpPa-1	195	113	0.214	1.25

Section S11. References:

1. Chong, J. H.; Sauer, M.; Patrick, B. O.; MacLachlan, M. J. *Org. Lett.* **2003**, *5*, 3823.
2. Kandambeth, S.; Mallick, A.; Lukose, B.; Mane, M. V.; Heine, T.; Banerjee, R. *J. Am. Chem. Soc.* **2012**, *134*, 19524.
3. a) Houk, R. J. T.; Jacobs, B. W.; El Gabaly, F.; Chang, N. N.; Talin, A. A.; Graham, D. D.; House, S. D.; Robertson, I. M.; Allendorf, M. D. *Nano Lett.* **2009**, *9*, 3413. b) Turner, S.; Lebedev, O. I.; Schroder, F.; Esken, D.; Fischer, R. A.; Tendeloo, G. V. *Chem. Mater.* **2008**, *20*, 5622. c) Suh, M. P.; Moon, H. R.; Lee, E. Y.; Jang, S. Y. *J. Am. Chem. Soc.* **2006**, *128*, 4710. d) H. R. Moon, J. H. Kim, M. P. Suh, *Angew. Chem. Int. Ed.* **2005**, *44*, 1261. e) Wahl, R.; Mertig, M.; Raff, J.; Selenska-Pobell, S.; Pompe, W. *Adv. Mater.* **2001**, *13*, 736. f) Stark, T. J.; Mayer, T. M.; Griffis, D. P.; Russell, P. E. *J. Vac. Sci. Technol., B* **1991**, *9*, 3475.
4. Henegar, K. E.; Lira, R. *J. Org. Chem.* **2012**, *77*, 2999.